Technical Report

TR-12-04

Temperature buffer test

Final report

Mattias Åkesson, Clay Technology AB

April 2012

Svensk Kärnbränslehantering AB
Swedish Nuclear Fuel
and Waste Management Co

Box 250, SE-101 24 Stockholm
Phone +46 8 459 84 00

ISSN 1404-0344
SKB TR-12-04
ID 1341331

Temperature buffer test

Final report

Mattias Åkesson, Clay Technology AB

April 2012

Keywords: Field test, Buffer, Bentonite, Temperature, Relative humidity, Water content, Density, Swelling pressure, Smectite composition, Thermo-hydro-mechanical processes, Numerical modelling.

Abstract

The Temperature Buffer Test (TBT) is a joint project between SKB/ANDRA and supported by ENRESA (modelling) and DBE (instrumentation), which aims at improving the understanding and to model the thermo-hydro-mechanical behavior of buffers made of swelling clay submitted to high temperatures (over 100°C) during the water saturation process. The test has been carried out in a KBS-3 deposition hole at Äspö HRL. It was installed during the spring of 2003. Two steel heaters (3 m long, 0.6 m diameter) and two buffer arrangements have been investigated: the lower heater was surrounded by rings of compacted Wyoming bentonite only, whereas the upper heater was surrounded by a composite barrier, with a sand shield between the heater and the bentonite. The test was dismantled and sampled during the winter of 2009/2010. This report is the final report and a summary of all work performed within the TBT project.

The design and the *installation* of the different components are summarized: the depositions hole, the heating system, the bentonite blocks with emphasis on the initial density and water content in these, the filling of slots with sand or pellets, the retaining construction with the plug, lid and nine anchor cables, the artificial saturation system, and finally the instrumentation.

An overview of the *operational conditions* is presented: the power output from heaters, which was 1,500 W (and also 1,600 W) from each heater during the first ~1,700 days, and then changed to 1,000 and 2,000 W, for the upper and lower heater respectively, during the last ~600 days. From the start, the bentonite was hydrated with a groundwater from a nearby bore-hole, but this groundwater was replaced with de-ionized water from day ~1,500, due to the high flow resistance of the injections points in the filter, which implied that a high filter pressure couldn't be sustained. The sand shield around the upper heater was hydrated from day ~1,500 to day ~1,800. The *sensors data* concerning temperature, relative humidity, total pressure, pore pressure, cable force and lid displacements is also summarized.

The dismantling operation was performed during a period from the end of October 2009 to the end of April 2010. One important goal with the dismantling operation was to obtain different types of samples for which two handheld coring machines was used: i) bentonite *cores* devoted for the so-called base program. These Ø50 mm cores spanned over the entire height of the bentonite blocks and were taken in four directions at 50 mm intervals; ii) large pieces of bentonite, so-called *big sectors*, were devoted for the hydro-mechanical and chemical characterization program and represented the entire radial distribution; and iii) so-called *end sectors*, i.e. pieces taken close to the rock or the lower heater. The experiment was also documented in different aspects: by measurements of the coordinate of different interfaces; verification of sensor positions and retrieval of sensors for subsequent function control; and by documentation of the operation through photography.

The base program, i.e. the determination of water content and density, was performed in parallel to the dismantling operation. The cores and end-sectors taken from the bentonite blocks were cut in smaller samples before the analysis, which in turn were analysed for water content and density.

The HM&C characterization program was launched subsequent to the dismantling operation. The main goal was to investigate if any significant differences could be observed between the field test material and the reference material. The following hydro-mechanical properties have been determined for the material: hydraulic conductivity, swelling pressure, unconfined compression strength, shear strength and water retention properties. The following chemical/mineralogical properties were determined: anion analysis of water leachates, chemical composition, cation exchange capacity and exchangeable cations, mineralogical composition, element distribution and microstructure, iron oxidation state. The retention tests, the CEC-determinations, the chemical analyses by ICP, and the mineralogical analyses by XRD and FTIR were performed on bulk samples as well as on a Na-converted fine fraction (< 0.5 μm). The latter fraction was subjected also to TEM analyses.

Several *THM modelling* tasks have been carried out since the beginning of the TBT project: from the initial scoping calculations, the predictions and the first evaluations of the field test, over the predictions and the evaluations of the two parallel mock-up tests, to the final modelling task of the field test after the dismantling of the field test. The final task was resumed after the dismantling

operation. The main part of this work has been numerical modelling of the field test. Three different modelling teams have presented several model cases for different geometries and different degree of process complexity. Two different numerical codes, CODE_BRIGHT and ABAQUS, have been used. The modelling also included different evaluations of experimental results with the aim to validate a number of data sets, and to assess the conditions in the tests prior to the dismantling operation. Finally, the validity of the material models has been assessed. This task has been a test of the different parts, or constitutive equations, of the material models, especially for the bentonite, for their ability to reproduce the experimental data

The test design of the TBT, especially regarding *the function of the sand-filled slots*, is discussed with the emphasis on the mechanical properties of the sand, the water injection, and the fractures observed in the bentonite blocks. For example, pieces from the inside of the upper rings fell out during the dismantling operation, whereas fairly horizontal fractures were found in virtually all blocks in the lower package.

Contents

1 Introduction

1.1 Background and objectives

The Temperature Buffer Test (TBT) is a joint project between SKB/ANDRA and previously supported by ENRESA (modelling) and DBE (instrumentation). The Temperature Buffer Test aims at improving the understanding of the thermo-hydro-mechanical (THM) behaviour of clay buffers at temperatures around and above 100°C during the water saturation transient, in order to be able to model this behaviour. The experiment was installed during the spring of 2003.

Apart from the general focus on THM behaviour, a number of additional aims were defined in 2007: i) gas migration, ii) retrievability of heaters, and iii) THMC-processes. The retrievablity of the heaters was facilitated by an inner sand-filled slot, which was denoted the sand shield, since it also would act as a thermal protection for the bentonite buffer. The gas test was not carried out since it was shown that the buffer around the sand shield was not sufficiently tight. In order to promote mineralogical alteration processes in the lower package, the thermal output from the lower heater was significantly increased at the end of 2007.

The test was dismantled during the winter of 2009/2010.

1.2 Outline of the report

The present report is a summary of all work performed within the TBT project. Detailed references are given to the reports from the different activities.

The different parts of the test design and the installation is described in Chapter 2. An overview of the operational conditions is given in Chapter 3 together with a summary of the different sensors data. The dismantling operation is described in Chapter 4. The analyses of density and water content in bentonite core samples obtained during the dismantling and the results from this program are presented in Chapter 5. The hydro-mechanical and chemical/mineralogical characterization programs and the results from these analyses are described in Chapter 6. A summary of all THM modelling work performed within the TBT project is given in Chapter 7. Finally, the test design of the TBT, especially regarding the function of the sand-filled slots, is discussed in Chapter 8.

2 Installation

2.1 General

The TBT was installed in the beginning of 2003. A detailed description of the installation is given in Johannesson et al. (2010). The summary presented below is primarily based on this report, which therefore is not mentioned in the text any further.

From the planning stage of the test a description of the foundation, artificial saturation system as well as the bentonite and sand materials was given by Thorsager (2002), whereas the data acquisition equipments and the data management system was described by Karlsson (2002) and Börgesson (2002), respectively.

2.2 Location

The test was installed in a full-scale KBS-3 deposition hole (No: DD0086G01) which originally was drilled in 1999 for the Canister Retrieval Test in the TASD-tunnel at the –420 m level in Äspö HRL. The deposition hole has a depth of about 9 m and the average diameter of the hole is 1,757 mm (Andersson and Johansson 2002). A characterization of this hole has been given by Hardenby (2002).

2.3 Heating system

Two heaters, made of carbon steel, have been used in the test (Figure 2-1). Each heater had a diameter of 0.61 m and a height of 3.00 m. The lower and the upper heater were denoted Heater 1 and Heater 2, respectively. The heaters were manufactured by Aitemin in Spain.

A feasibility study was performed prior to the installation (García-Siñeriz and Fuentes-Cantillana 2002). Detailed information of the installed heating system is given in Johannesson et al. (2010).

2.4 Bentonite blocks

The heaters were surrounded by a bentonite buffer, which was installed as 12 rings and 4 cylinders. These blocks were made of a sodium dominated Wyoming bentonite produced by American Colloid Company with the commercial designation MX-80. The water content was increased to around 17.5% by use of tap water and was compacted to two different shapes; ring shaped blocks, which were placed around the upper heater and massive cylindrical blocks, which were placed above and under the heaters. The blocks were uniaxially compacted in a rigid form to an outer diameter of about 1,650 mm and a height of about 500 mm. The inner diameter of the ring shaped blocks was about 1,070 mm. The cylindrical blocks were also used around the lower heater after machining of a hole with a diameter of about 630 mm in the central part of the block. In order to have similar average density everywhere (including the gaps), the two types of blocks were compacted to different densities. The initial average weight, water content (i.e. the water-solid mass-ratio), density, degree of saturation and void ratio of the used blocks are listed in Table 2-1.

Some blocks of brick size were installed on top of Heater 1. These blocks had a water content of about 15.1% and a bulk density of about 2,030 kg/m^3.

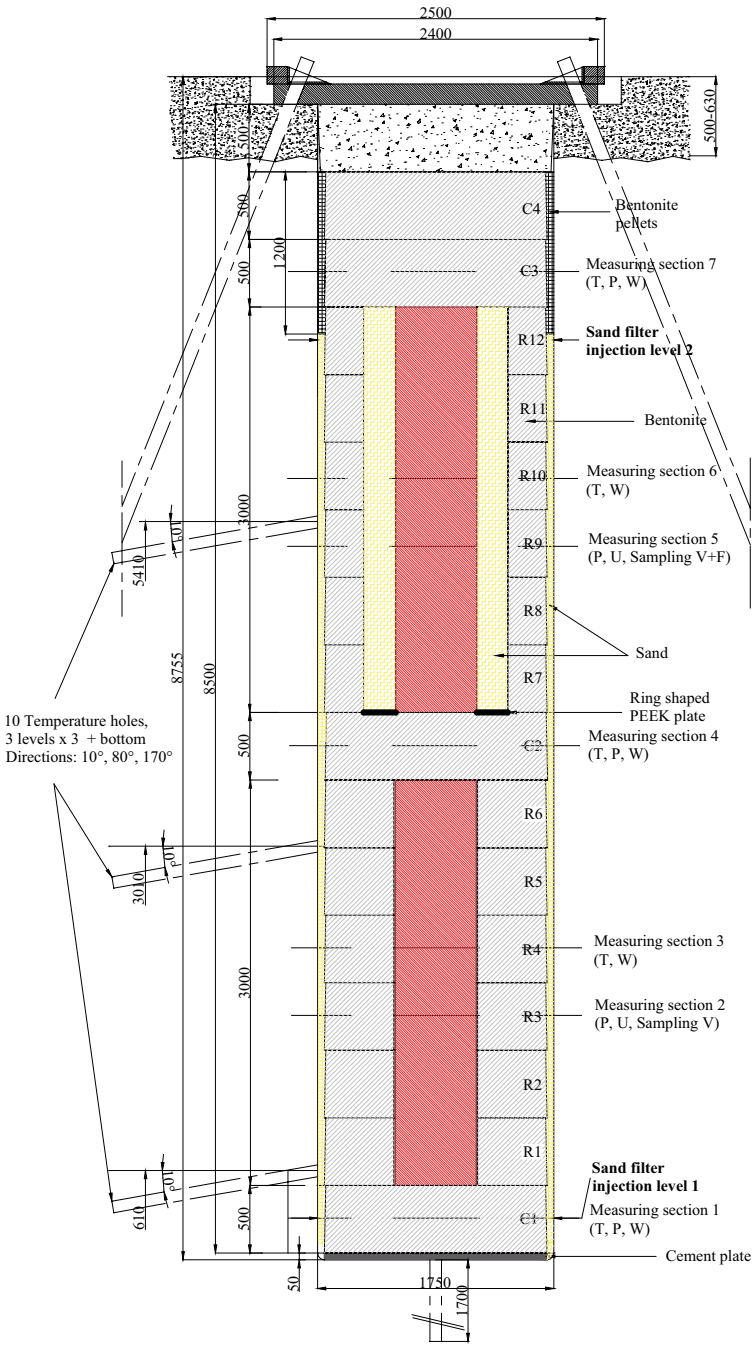

Figure 2-1. *Design of the TBT experiment (T = temperature; P = total pressure; U = pore pressure; W= relative humidity; V = vessel; F = filter tip).*

Table 2-1. Basic properties for blocks used in TBT.

Block No.	Weight (kg)	Water content (%)	Bulk density (kg/m^3)	Degree of saturation	Void ratio
C1	2,104	17.5	2,015	0.784	0.622
R1	2,116	17.5	2,008	0.776	0.626
R2	2,122	17.5	2,007	0.775	0.628
R3	2,124	17.7	2,004	0.778	0.632
R4	2,108	17.7	2,006	0.779	0.631
R5	2,130	17.4	2,005	0.772	0.629
R6	2,108	17.4	2,009	0.774	0.625
C2	2,112	17.5	2,008	0.776	0.627
R7	1,256	17.5	2,066	0.838	0.581
R8	1,266	17.6	2,075	0.849	0.575
R9	1,266	17.3	2,081	0.848	0.567
R10	1,250	17.7	2,080	0.857	0.573
R11	1,254	17.5	2,077	0.850	0.572
R12	1,258	17.6	2,075	0.849	0.575
C3	2,142	17.5	2,010	0.778	0.625
C4	2,084	17.6	1,997	0.768	0.637

2.5 Sand and pellets

The filling of the outer gap with sand was made after the emplacement of each bentonite block. Sand was filled up to about mid height of block R12. The total amount of sand used for filling the outer gap was about 3,984 kg. The average density of the sand filling can be calculated to 1,729 kg/m^3 for a hole-diameter of 1,757 mm.

When the blocks around the upper heater were put in place the gap between the heater and the bentonite buffer was filled with sand. The sand was compacted by hand. The total weight of the sand was about 3,357 kg. The average dry density of the sand filling was after the installation about 1,820 kg/m^3.

The upper part of the gap between the bentonite and the rock wall was filled with pellets of bentonite (MX-80) in order to seal off the sand filling below. The bentonite pellets had an initial water content of about 16%. The width and the length of each pellets was about 16.3 mm and the maximum thickness was about 8.3 mm. The bulk density of the separate pellets varied between 1,970 and 2,110 kg/m^3. The expected bulk density of the filling of pellets was between 1,100 and 1,300 kg/m^3. The total amount of pellets was about 745 kg. The average density of the pellets filling can be calculated to 1,263 kg/m^3 for a hole-diameter of 1,757 mm.

2.6 Retaining construction

The lower part of the buffer was placed on a concrete foundation. The upper part was retained by a 0.5 m thick concrete plug. This was in turn kept in place by a 150 mm thick steel lid, which was anchored to the rock with nine anchor cables. A description of the design of the plug and the anchoring was given prior to the installation by Bäck (2002).

2.7 Artificial saturation

The test was supplied with water through the sand filter and was fed through 8 injection points, four in the lower part and four in the upper part. In addition, to enable the supply of water to the upper part of the buffer, a filter mat was located between the two uppermost blocks. This mat was fed through two injection points. A system for artificial saturation by which the injection points could be pressurized was located in the gallery. This consisted of a pressurized water tank equipped with a differential pressure sensor used for monitoring of the water level in the tank. The water pressure was monitored downstream in the main tube as well as in each tube leading to the filter tips in the sand filter. The latter sensors were installed 562 days after the test was launched. The pressure in the sand filter could thereafter be monitored through non-pressurized filter tips.

2.8 Instrumentation

The bentonite blocks were instrumented for measurement of temperature, total pressure, pore pressure and relative humidity (Figure 2-1). The temperature was also measured in and on the heaters, as well as in the surrounding rock. A compilation of the number of sensors located in or adjacent to the bentonite and the sand filled volumes are given in Table 2-2. Load cells were used for measurements of cable forces, and displacement sensors were installed for monitoring the movements of the lid. A number of additional installations enabled different types of monitoring and fluid sampling through filter tips and vessels. For instance, the gas in the sand shield has been sampled and analysed (see Goudarzi et al. 2007b). Finally, a number of fiber optic pressure and temperature sensors have been installed, tested and evaluated by DBE Technology. Information about these sensors was given in Goudarzi et al. (2006, 2007a). Data from these sensors are not maintained by SKB.

A paper which described the instrumentation was presented by Sandén et al. (2007).

Table 2-2. Numbers of sensors in different sections.

Section	Thermo-couple	Wescor RH sensor	Rotronic RH sensor	Vaisala RH sensor	Geokon total pressure	Geokon pore pressure
Cylinder 1	14	2	2	1	3	–
Ring 3	–	–	–	–	9	4
Ring 4	25	3	3	4	–	–
Cylinder 2	14	2	2	1	3	–
Ring 9	–	–	–	–	9*	3
Ring 10	19	3	3	2	–	–
Cylinder 3	14	2	2	1	3	–
Sand shield	6	–	–	2	–	1
Rock surface	10	–	–	–	2	–
Heater 1 surface	11	–	–	–	–	–
Heater 2 surface	11	–	–	–	–	–

* One sensor located at the section of Ring 7”.

3 Operation and sensors data

3.1 General

The operation of the test and the results from the installed instruments have been continuously evaluated and reported. In total, 13 sensors data reports have been published (Goudarzi et al. 2003, 2004a, b, c, 2005a, b, c, 2006, 2007a, b, 2008a, b, 2010). The summary presented below is primarily based on these reports, which therefore are not mentioned in the text any further.

3.2 Overview of the operational conditions

The operational conditions have evolved during the course of the test, see Figure 3-1.

The power output from each heater was 1,500 W during the first three years. The termination of the Canister Retrieval Test (CRT) at the end of 2005 implied a minor decrease in the background temperature around TBT. The power output was therefore increased to 1,600 W from each heater in June 2006. This level was kept until the end of 2007, when the output was significantly rearranged: the power output from the lower heater was increased to 2,000 W, whereas from the upper heater it was decreased to 1,000 W. This condition was sustained until August 2009 when the heating was terminated.

The artificial saturation through the sand filter was also changed during the test period. The sand filter was initially only pressurized through the lower injection points, while the upper were open to the atmosphere. After one year, the upper injection points were also pressurized while none of the injection points were open to the atmosphere. Equipment for measuring pressure at each injection point was installed in October 2004. After that, at least one out of eight injection points were closed and used for monitoring of the actual pressure in the sand filter. The filter mat between Cylinder 3 and Cylinder 4 was activated at the end of 2005. The water quality was changed in April 2007 from

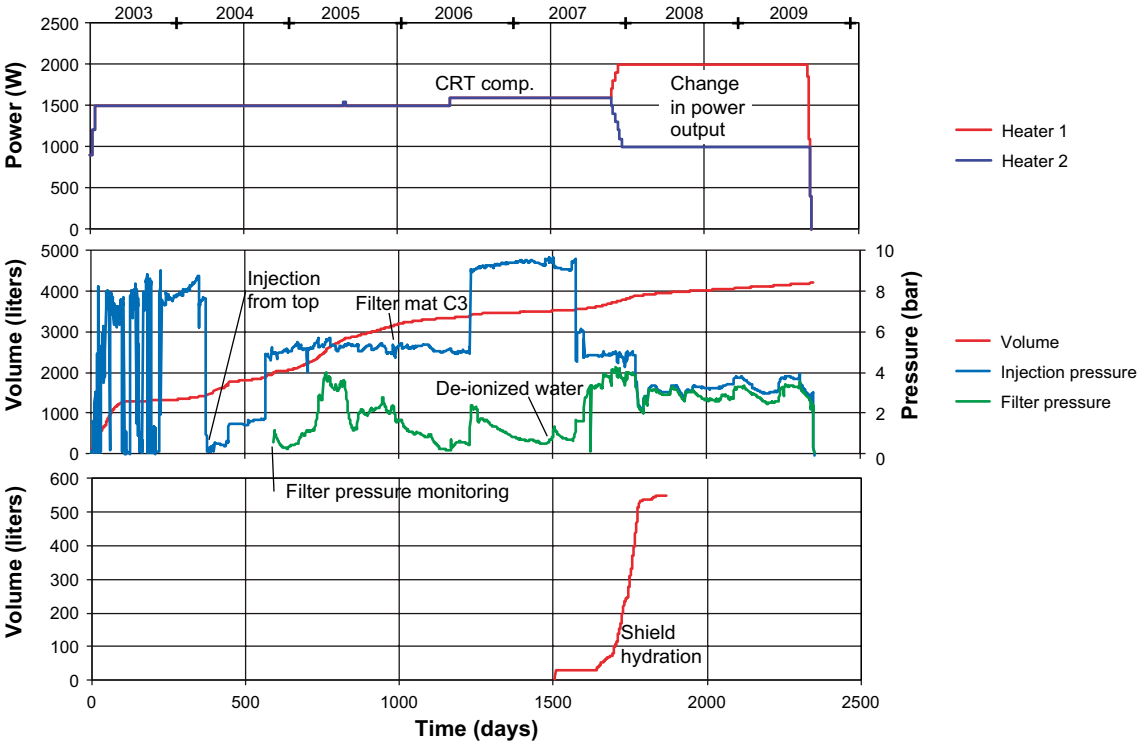

Figure 3-1. *Timeline of major events regarding power output (upper), filter injection system with total injected volume and pressures (middle); and shield hydration with total injected volume (lower).*

formation water to de-ionized water. The motive for this was that the injection points in the sand filter had exhibited a high flow resistance. The total injected water volume had reached 4.2 m^3 when the water injection was terminated. This volume exceeded the calculated available pore volume with 1.5 m^3. This discrepancy appears to be caused by a water leakage, possibly into the rock.

The sand shield around the upper heater was hydrated with de-ionized water during the second half of 2007 and the beginning of 2008. The aim of this was to facilitate hydraulic tests and gas injection tests through the upper buffer package. In total, approximately 540 liters of de-ionized water was injected. A water leakage was detected at the lid at the end of the shield hydration and during the subsequent hydraulic test. The apparent lack of correlation between the injection pressure and the filter pressure suggested that the sand filter was not involved in this leakage. Instead there appeared to be a direct route from the sand shield to the upper part of the pellets filling. This was supported by the traces of a large shearing event in Ring 12 and Cylinder 3 which was observed during the dismantling (see section 4.4).

3.3 Temperature

In general, the temperature in the bentonite exhibited consistent trends and reached maximum levels after about 200 days, except for the inner part of Cylinder 2 where the maximum temperature was reached after only about 40 days. After this, the temperature levels in the bentonite were fairly constant until the termination of CRT at the end of 2005, when a minor but general decreasing trend could be observed. In order to compensate for this loss, the power output from the TBT heaters was increased to 1,600 W. As a consequence to this adjustment, the temperature conditions were restored.

In contrast to the fairly stable temperature levels in the bentonite, the upper heater displayed decreasing temperatures already 60 days after start, when it was 166°C. In the beginning of 2006 it had decreased to 144°C. This indicated that the thermal conductivity of the shield had increased. The hydration of the sand shield also influenced the conditions around the upper heater, and this is reflected by some of the temperature data. The temperatures on the upper heater tended to decrease whereas the temperatures in Ring 10 tended to increase.

The major change in power output at the end of 2007 significantly altered the thermal conditions in the experiment. The temperature on the mid-section of the lower heater increased from 139 to 158°C. The corresponding decrease for the upper heater was from 134 to 89°C. Slightly lower temperatures prevailed until August 2009, when the mid-section temperatures on the lower and the upper heaters were 152°C and 86°C, respectively (Figure 3-2).

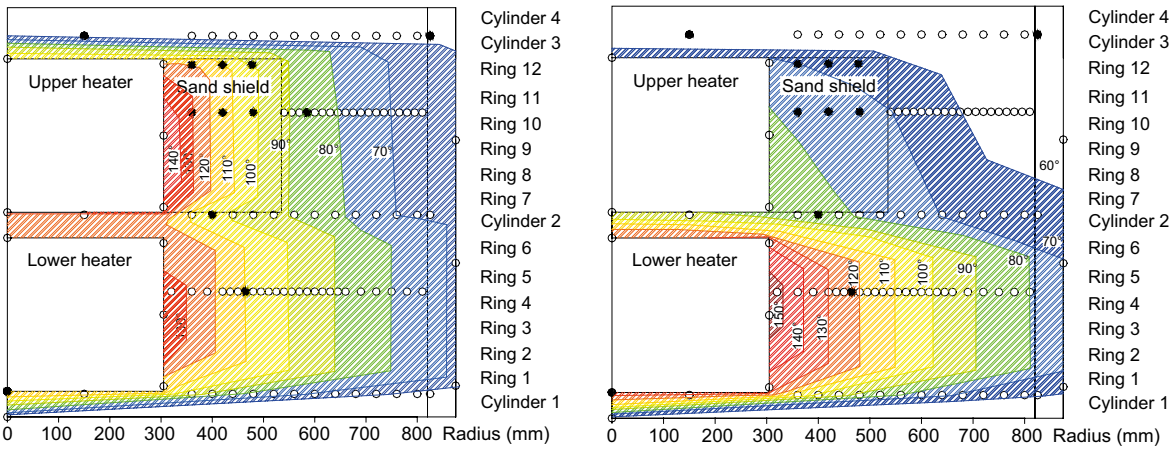

Figure 3-2. *Temperature distribution on January 1, 2007 (left) and August 16, 2009 (right). Rings indicate sensor positions. Filled rings indicate sensors out of order.*

3.4 Relative humidity

The hydration of the bentonite is reflected by the increasing RH values recorded by the capacitive sensors. The initial values spanned from 69 to 75%. Most RH sensors displayed a fairly steady increase from the start. In the outer part of most blocks, the RH values reached 100% within 240 days (see Figure 3-3, it should be noted that these occasions of vapor saturation cannot generally be equated with water saturation, see Åkesson et al. 2012b). Exceptions with decreasing RH-values which fell below the initial level were displayed by the innermost sensor in Ring 4, the two innermost sensors in Cylinder 1 and the two sensors at the sand shield – bentonite interface of Ring 9 and 10. The last sensor to reach 100% was the innermost sensor in Cylinder 1. This occurred around day 1,700 and was probably influence by the increasing power output at that time.

The data recorded by the psychrometers was limited to an interval in suction between 6 and 1 MPa, which approximately corresponds to RH levels above 95%. Consequently, these sensors did not respond until conditions close to vapor saturation were established. In general, all psychrometers displayed decreasing trends in suction.

A major exception was the suction increase of the two outermost psychrometers in Ring 10 after day 225. This increase was correlated with a general decrease in stresses in parts of Ring 9, and was most likely caused by a shortage in water supply. The trend was reversed when the water injection through the upper tubes was initiated at day 377 (see also section 7.4).

3.5 Total pressure

The total pressure generally displayed a fairly rapid buildup from the start. For example, after the first 400 days, all sensors showed stresses above 5 MPa, except the two innermost sensors in Ring 3, all the radial sensors of Ring 9, and all sensors in Cylinder 3. The slow buildup of stresses in Cylinder 3 appears to be a consequence of the pellets filling around this and the adjacent blocks, which meant that the access of water was limited. The buildup of stresses advanced rapidly with the activation of the filter mats at around day 1,000.

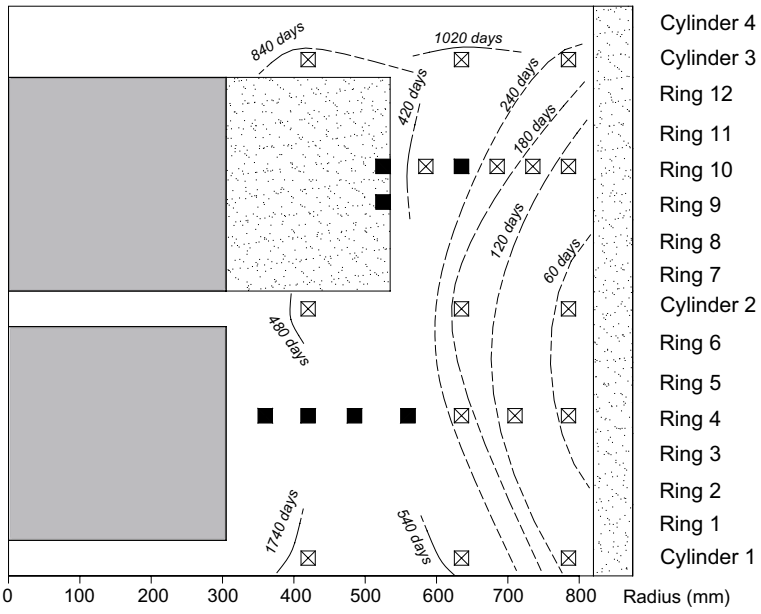

Figure 3-3. *Compilation of occasions when capacitive sensor signals showed RH ≈ 100% (Vaisala and Rotronic), and psychrometers (Wescor) gave significant results (RH > 95%). Boxes are sensor positions. Filled boxes indicate sensors that failed prior to vapour saturation. Some data indicate that the four capacitive sensors closest to the rock wall in Ring 4 reached 100% before day 100 (Åkesson et al. 2012b).*

A compilation of total pressures from around day 1,200 is shown in Figure 3-4. Higher pressure levels generally occurred in the outer parts of the experiment, except for the upper cylinder. The condition in the Cylinder 1 and 2 were quite isostatic, while the sections around the heaters were characterized by deviatoric stresses, with relatively lower radial stresses.

At around day 1,500 the stresses in almost all bentonite blocks had largely stabilized. The subsequent activities had some influence on the pressures. The hydration of the sand shield resulted in a decrease in total pressure in Ring 9. This appears to be an effect of swelling of the buffer into the sand shield.

The change in power output also influenced the total pressures. The total pressures around the lower heater (Ring 3) first displayed a minor increase, after which they decreased slightly more than the initial increase. The cause of the general pressure decrease in Ring 9 observed at the end of 2007 is difficult to identify, since the decrease in power output coincided with the shield hydration. A few months after these events the pressures appears to have recovered to their original levels. A comparison of axial pressures and cable forces is shown in Figure 3-6.

Three total pressure sensors in Ring 3 (PB208, 212 and 213) displayed increasing values during the last 500 days, which implies that a water uptake still took place at that time. The relatively low total pressures that were measured in the inner part of Ring 3 (Figure 7-2) can also be interpreted as the bentonite was not totally water saturated.

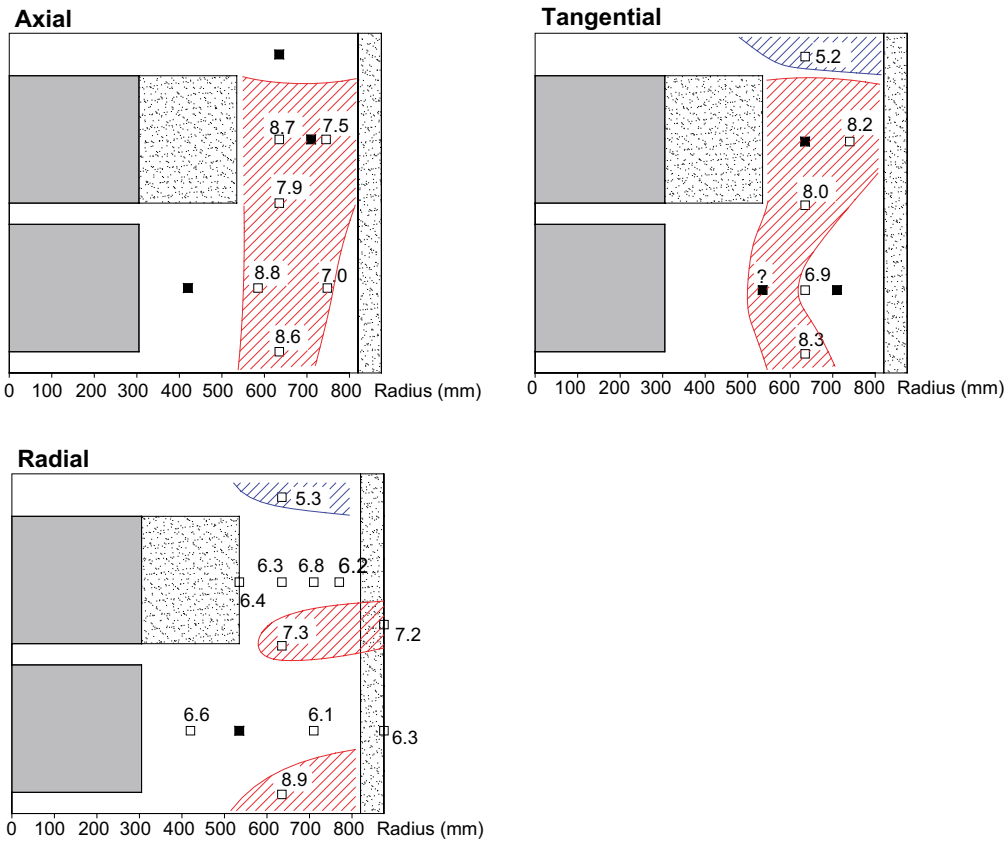

Figure 3-4. *Total pressure distribution at July 1, 2006. Values in MPa. Boxes are sensor positions. Filled boxes indicate sensors out of order. Levels above 7 MPa marked red; below 6 MPa marked blue. Tangential pressure sensor in Ring 3 with a question mark showed values higher than 7 MPa at an early stage.*

3.6 Pore pressure

Significant measured pore pressures were first observed around day 700–800, a period which coincided with relatively high filter pressures (Figure 3-5). The outermost sensors (at 785 mm radii) in Ring 9 as well as in Ring 3 responded at that time. In Ring 9, the registered pore pressure was highly correlated with the filter pressure. In contrast, the pore pressure in Ring 3 was lower and displayed a more stable trend.

A second event with beginning responses from the pore pressure sensors occurred concurrently with the general increase of the power output (1,500 → 1,600 W), at day 1,171. At this time the two additional sensors in Ring 9 (at 635 and 710 mm radii) began to display trends correlated with the filter pressure, although at a higher level.

A third response occurred at the same time as the major increase in power output (1,600→ 2,000 W), at around day 1,700. At that time the three additional sensors in Ring 3 (at 420, 535 and 635 mm radii) began to display significant levels, although with different trends. The concurrent shield hydration led to a temporary reduction of the pore pressure in the bentonite in Ring 9.

3.7 Cable forces and lid displacements

The cable forces and the lid displacements have evolved in parallel. The final reading just before the dismantling showed that the displacement was 24 mm, whereas the total cable force was 14 MN. If can be noted that these quantities had reached 50% of their final values already after approximately 500 days.

The evolution of the cable forces are shown in Figure 3-6 after conversion to pressures under the assumption that the forces are evenly distributed over the entire test hole area. Moreover, the results from axial pressure sensors located at radii 585–635 mm are also shown. A fairly clear-cut arrangement can be observed, which suggests that the vertical forces were predominantly transferred in a section corresponding to the buffer rings around the upper heater. The stress levels around the heaters and in the lower cylinders have during the test period been significantly higher than in the upper part of the experiment. This difference has however decreased during the test period.

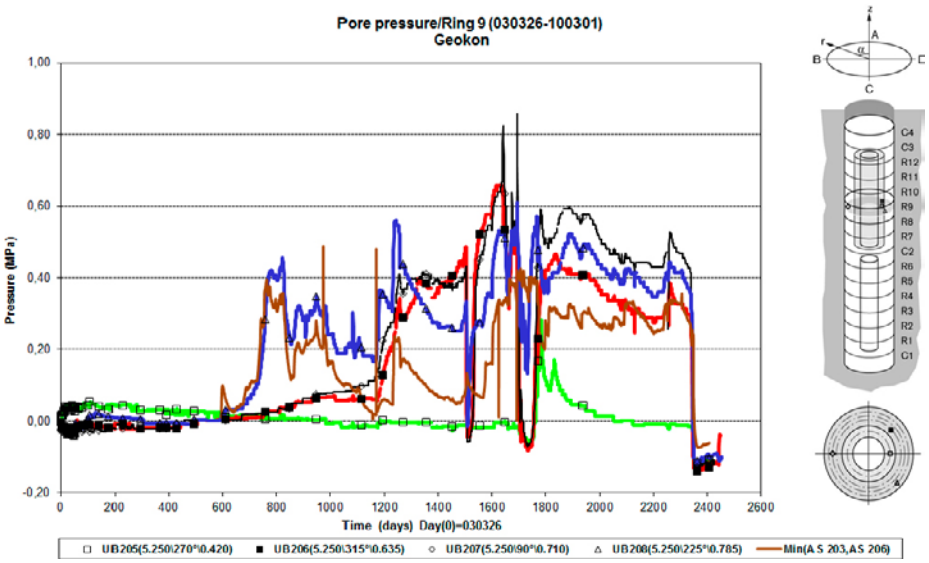

Figure 3-5. *Evolution of pore pressure in Ring 9 (symbols) and filter pressure (brown line).*

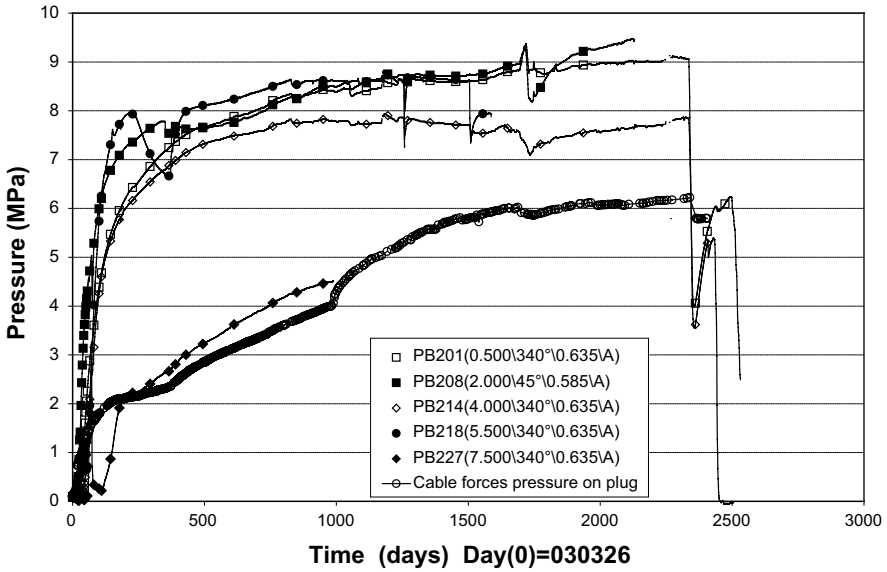

Figure 3-6. *Axial pressure measured in different sections. Cable forces are shown as pressures, assuming an even distribution over the test hole area (2.4 m^2).*

4 Dismantling operation

4.1 General

The test was dismantled and sampled during a period from the end of October 2009 to the end of April 2010. This operation has been described in detail by Åkesson (2010). The summary presented below is primarily based on this report, which therefore is not mentioned in the text any further.

4.2 Goals

One important goal of the dismantling operation was to obtain different types of samples for the various subsequent analyses. Bentonite cores were devoted for the so-called base program, in which the bentonite was analysed for water content and density. Large pieces of bentonite, so-called big sectors, were devoted for the HM&C (hydro-mechanical and chemical) program. Finally, there was an interest to obtain different types of interface samples in which bentonite were in contact with sand, iron or concrete.

A second goal was to investigate the retrievability of the upper heater, as facilitated by the possibility to remove the surrounding sand shield.

Finally the experiment was documented in different aspects: measurements of the coordinate (height or radius) of different interfaces (between bentonite blocks and between bentonite and sand); verification of sensor positions and retrieval of sensors for subsequent function control; and by documentation of the operation through photography.

4.3 Method

The main method to sample and partition the bentonite blocks was with the use of two handheld coring machines used in parallel. The inner and the outer diameter of the coring machine were 50 and 66 mm, respectively. The plan was to take cores that spanned over the entire height of the bentonite blocks, i.e. approximately 500 mm. For each block a coring scheme was specified according to which cores were to be taken in four directions at 50 mm intervals. A plywood template was produced to specify these coring positions in the field. The same directions[1] were aimed for in all blocks: 32, 122, 212 and 302° (Figure 4-1). One reason for choosing these angles was that they would coincide with the orientation of the lid of the lower heater. It was also found that these angles were generally free from instruments, and also that it would be beneficial to keep the same angles in all blocks for simplicity.

In addition to the sampling of cores, the plan was to "cut" out two so-called big sectors from each block representing the entire radial distribution in two directions: 32 and 212°. These were given a width of at least 100 mm. In order to obtain samples close to the rock wall and the lower heater, so called end sectors were taken. In the lower part of the experiment, it was found to be beneficial to make a circular stitch drill around the heater which enabled the sampling of suitable pieces close to the heater.

All samples were packaged in evacuated aluminium laminate foil bags. The top surface of the bentonite was covered with a rubber mat during all nights, weekends and holydays throughout the dismantling operation.

[1] Directions (or azimuths) were defined as counterclockwise with zero in the direction of the end of the TASD tunnel.

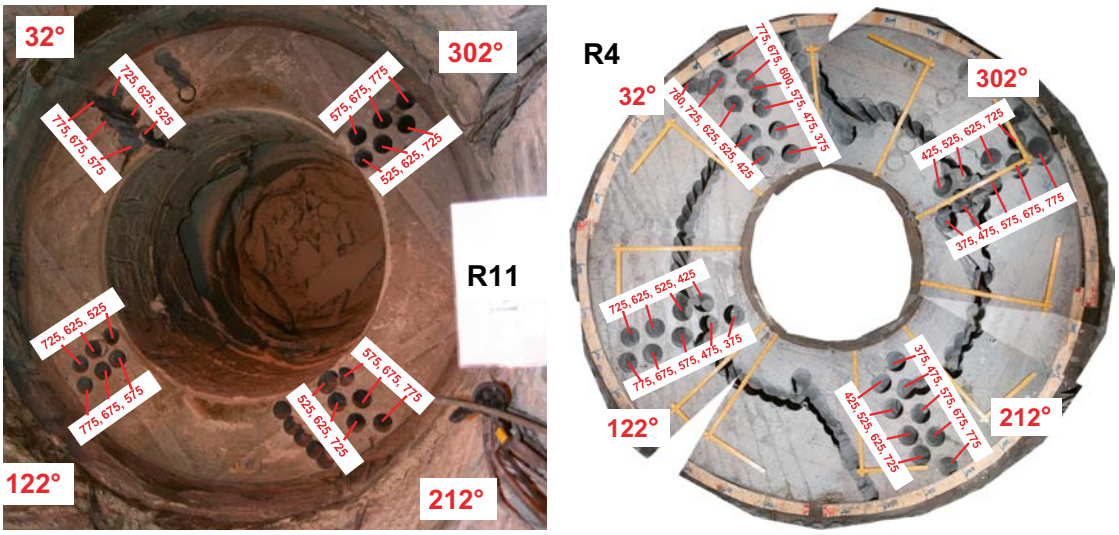

Figure 4-1. *Cores of Ring 11 (left) and Ring 4 (right).*

4.4 Upper package (plug to Ring 7)

The actual dismantling operation began with the removal of the plug. The plan was to unload the cables through releasing three cables at a time with only a few mm in an iterative scheme using hydraulic jacks. This was however found to be very difficult, and instead the cables were released completely one at a time. Leveling performed prior and subsequent to the unloading showed that the plug had moved approximately 14 mm upwards during the unloading. After the unloading, the steel ring, the lid and finally the concrete plug was lifted from the deposition hole.

In general, the sampling of Cylinder 4 and 3 was performed according to the plans with cores and big sectors, but also with a cylindrical centre piece which was created through circular stitch drilling above the lid of Heater 2. This was only a rehearsal for the real sampling on top of Heater 1.

A number of observations at Cylinder 3 and Ring 12 have been interpreted as traces of a large shearing process (Figure 4-2). At the top of Cylinder 3 it was observed that the surface and the filter mat were broken at some locations in the outer parts between 120 and 270 with protruding areas. At the top of Ring 12: two “shelves” with approximately 5 cm high inclined lateral sides were found at around 0° and between 160 and 270°. The inclination of the lateral side at the shelf in the 350° direction was measured to approximately 65° in relation to the horizontal plane. The corresponding inclination in the 200° direction was measured to approximately 72°. The directions of the observed shelves between 160 and 270° coincide with the slots in which the leakage was observed during the shield hydration (see Section 3.2). Together with the results from the levelling these observations suggest that the upward swelling of Ring 12 had sheared the outer parts of Cylinder 3.

The plan was to remove the sand in the shield with an industrial vacuum cleaner. It was found that the sand had to be loosened before it could be removed. This was first achieved with a hammer drill (Hilti), and later on (deep down) with the core machine. The difficulties of removing the sand increased with depth. It was not until only approximately 5 cm of sand remained in the bottom that it was possible release the heater. This was achieved with a front loader which could rock the heater sideways. This phase of dismantling showed that the sand could be fairly easily removed with a proper loosening action, and also that the canister could be loosened from the grip of the swelling bentonite without too much difficulty.

Soon after the sand and the heater had been removed, it was noticed that some material from the bentonite rings fell out. This fallout became more severe with time, especially in Ring 10 – Ring 7, which complicated the core sampling in this rings. The positions of the sampled cores were in some cases modified in angle, and the number of cores was reduced in some cases. The sampling of big sectors was also affected by the fallout, and the measurements of the radial position of the interfaces were also complicated.

Figure 4-2. *Shelfs of top surface of Ring 12 indicating shearing. Left: in 350° direction inclination approximately 65° in relation to the horizontal plane; right: in 200° direction inclination approximately 72° in relation to the horizontal plane.*

During the course of dismantling of the upper package it was found that the total pressure sensor PB226 was not installed at the level of Ring 9 as specified earlier, but rather at the level of Ring 7. The injection points in the sand shield CS202 and CS203 were of interest since these points have shown very high flow resistance. It was found that these points were surrounded by bentonite. All bentonite and sand down to Cylinder 2 was removed before December 23rd. At this time the PEEK-plate was also removed, after which the Cylinder 2 was covered with a rubber mat.

4.5 Lower package (Cylinder 2 to Cylinder 1)

The plan was to take a 200 mm high undisturbed centre sample from Cylinder 2, on top of the lid of Heater 1. This operation followed a fairly complex scheme, and the sampling was enabled by making a circular stitch drill at a 275 mm radius. Cores and big sectors could be taken on the outside of this circle in the usual directions. On the inside, however, the sampling was limited to cores taken to a depth of 300 mm in the 32 and 212° directions. In the end, all material on the outside of the circle was removed, leaving only the central sample on top of the heater lid. The sample was strapped to the lid and could be lifted from the deposition hole. This was placed in an evacuated aluminium foil bag which in turn was placed in a special fabricated container.

The coring in Ring 6 could be implemented as planned, although the sampling in the 122° direction was interfered by the presence of the power cables. During the removal of the material in Ring 6 it was noticed that the material was very restrained by the swelling pressure, and it was therefore difficult to remove the material without damage, especially close to the heater. It was also noticed that some bentonite was stuck to the heater, possibly associated with the welding at the top end.

A circular stitch drill approximately 150 mm from the heater was made in all rings from Ring 5 downwards (Figure 4-1). This made it easier to loosen and remove the big sectors and the remaining material without damage. Additional sampling from the inside of the circular stitch drill was carried out during the removal of material in Ring 4 and Ring 3. During this operation, the samples were put in evacuated aluminum laminate foil bags as well as in plastic barrels which were flushed with nitrogen gas before they were closed. In the case of the samples taken from Ring 3, the evacuation of the bags was made in the deposition hole in order to minimize the exposure to atmospheric oxygen.

Coming down to Ring 1 a second attempt to take an undisturbed bentonite iron interface sample was made. This was performed with a circular stitch drill, similar to the ones used at the rings above. No cores were however taken on the inside of the circle. The cylindrical bentonite piece attached to the heater was reinforced with mounted wooden planks and straps. The heater was thereafter lifted out of the deposition hole, and subsequently put in a cradle. The attached bentonite was covered with plastic foil.

The sampling of the Cylinder 1 was commenced immediately after the lifting of Heater 1. The sampling and the removal of the bentonite proceeded as planned. Four samples of bentonite-concrete interfaces were taken at the end of the operation. These were taken with a 76 mm diameter coring machine at an inclination of approximately 30°. All bentonite material was removed on April 20th.

4.6 General observations

The top surfaces of bentonite blocks, heaters, peek plate and concrete bottom plate were levelled during the dismantling. In addition, the outer and inner radii of the bentonite blocks were measured in different directions. Graphical representations of all these measurements are shown in Figure 4-3. These pictures also illustrate the traces of shearing of Ring 12 and Cylinder 3 mentioned above.

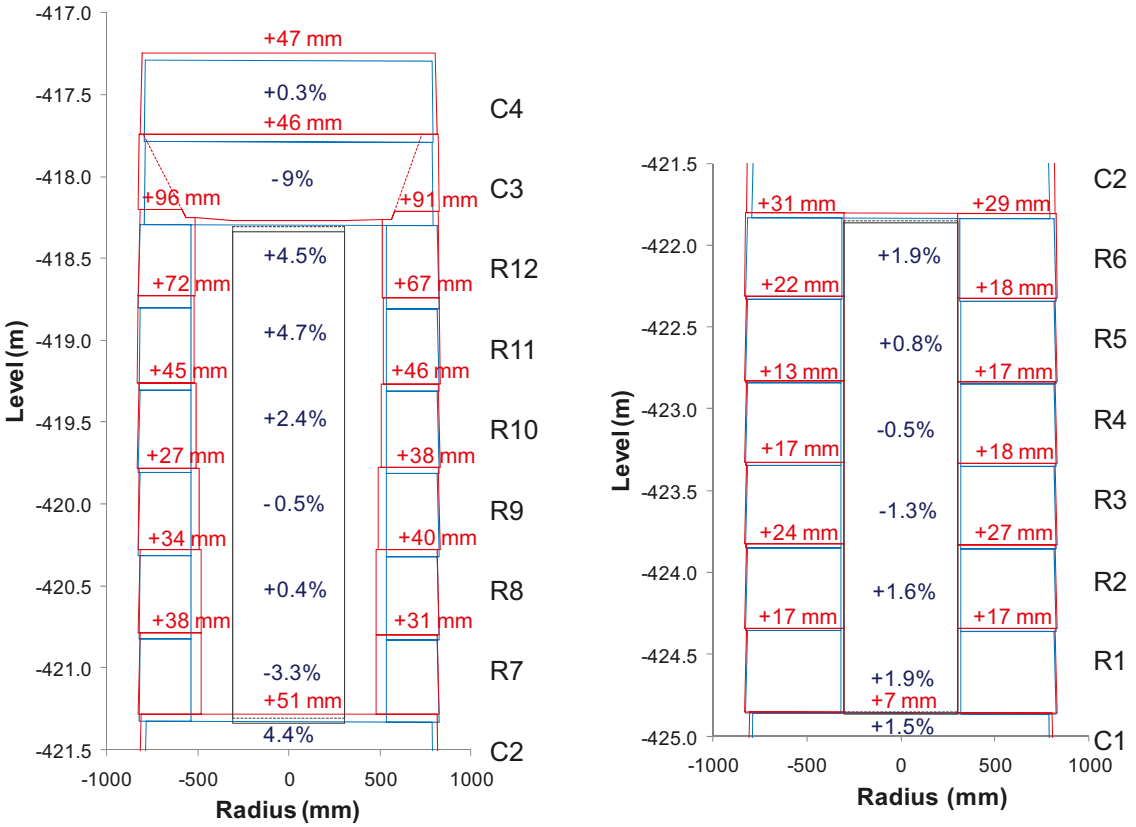

Figure 4-3. *Contours of bentonite blocks at installation (blue lines) and at dismantling (red lines). Heaters are shown with black lines (solid for installation and dotted for dismantling) Absolute changes in height (red numbers), and relative changes in thickness (blue numbers) are shown for each block in the upper (left) and lower (right) package. The levels on the left and the right side of each block correspond to the 0° and 180° directions, respectively.*

The joints between the different blocks only displayed a marginal attachment during the dismantling operation. The removal of remaining material after the sampling of each block followed these original joints. Large quadratic shapes could be seen on several blocks (see Figure 4-1). These shapes are "negative" marks of the grooves on the bottom face of the blocks above which were made in order to facilitate the removal of the lifting straps used during the installation of the blocks.

Fairly horizontal fractures were observed in virtually all blocks in the lower package, i.e. from Cylinder 2 and downwards. This affected the sampling so that the cores in almost all cases came up as two or three pieces.

4.7 Preparation of bentonite/iron interface sample

A number of different actions were performed in order to obtain a manageable interface sample from the material from the inner part of Ring 1 which was attached to Heater 1. The bentonite was first partitioned with a hand saw so that approximately 80° of material remained on the heater. A gas sample was subsequently taken from the interior of the heater, which showed that the volumetric concentration of hydrogen was in the order of 8–9% with an absolute gas pressure of 0.75 bar. The heater was therefore flushed repeatedly with nitrogen before the heater was considered to be safe for sawing. This operation was performed with the saw for canister components at the Canister Laboratory in Oskarshamn. The heater was cut perpendicular to the heater axis approximately 2 dm from the attached bentonite piece. This specimen was wrapped in several layers of plastic foil.

4.8 Sensor function control

During the course of the dismantling operation a number of sensors were retrieved. These sensors have subsequently been tested at different operational conditions. This activity has been described in detail by Goudarzi et al. (2010).

Thermocouples were tested *in situ* in the deposition hole at two temperatures. Three different types of pressure sensors (Druck; and Geocon, total and pore pressure sensors) were exposed to several pressures levels. Finally, a few capacitive relative humidity sensors (Rotronic and Vaisala) were exposed to three different relative humidities.

These tests generally showed good results for the thermocouples, the Geokon pore pressure sensors and the Druck pressure sensors. In contrast, the Geokon total pressure sensors and the capacitive relative humidity sensors in general exhibited a function outside the stated specifications. For instance, the linear errors for the total pressure sensors were generally 5–10%.

Precipitates from one of the filter tips in the sand filter was analysed with X-ray diffraction. This analysis indicated that the sand was cemented by calcite.

5 Density and water content at the end of test

5.1 General

The cores sampled during the dismantling operation have been analysed for water content and density. These analyses were performed in the bentonite laboratory at Äspö HRL. This characterization program has been described in detail by Johannesson (2010). The summary presented below is primarily based on this report, which therefore is not mentioned in the text any further.

5.2 Method

The samples taken from the buffer were split up in smaller pieces before determining their water content and density. The split was made with a band saw according to the following plan:

- In two directions (122°, 302°) samples were taken with a radial distance of 5 cm at one depth measured from the top of each block.
- In one direction (212°) samples were taken with a radial distance of 2.5 cm at one depth measured from the top of each block.
- In one direction (32°) samples were taken with a radial distance of 5 cm at five depths measured from the top of each block,
- The end sectors of the blocks taken close to the rock wall or the heaters were cut in samples with a radial thickness of 1 cm.

The water content of the samples was determined by drying each sample at a temperature of 105°C for 24 hours. The water content was calculated as the ratio between the mass-loss during drying, and the dry mass of the sample. The bulk density of the sample was determined by measuring the mass of the sample; and the volume of the sample, through submerging the sample in paraffin oil.

Measured values on water content and bulk density for each sample were used to calculate the dry density, the void ratio and the degree of saturation.

5.3 Results

Very small differences in the measured, as wells as in the calculated results, could be found for the four directions in all blocks, except for Ring 6. The 122° direction in this latter block showed a lower density and a higher water content compared to the other three directions. This could be a consequence of the cuts made across the block in order to make room for the power cables. The remaining voids of these cuts were filled with bentonite powder which was compacted in place.

The water content in all blocks had increased at all measuring points compared to the initial values.

The dry density of the buffer has decreased in comparison to the initial state in all the blocks except for the inner parts of Ring 1-6 close to the heater where a small increase in density were found. The decrease of density was most pronounced for the buffer close to the sand filter, or the rock wall in the case of the upper blocks.

The degree of saturation was 100% in the outer parts of all blocks close to the sand filter or the rock wall in the case of the upper blocks. In the innermost parts of the blocks in the lower package (Cylinder 1 – Ring 6) the degree of saturation was about 95%. The lowest saturation degrees in Ring 1-6 were found approximately 70 mm from the heater surface (Figure 5-1). In the central parts of Cylinder 2 the degree of saturation was about 94. The corresponding value for Cylinder 3 and Cylinder 4 was 97% and 92%, respectively. Finally, in Ring 7-12 the saturation degree was close to 100% in all parts of the buffer.

Contour plots of measured results

Contour plots of the measured and calculated variables water content, dry density, degree of saturation and void ratio were made using an interpolation program. Since the water uptake apparently was quite axisymmetric, all data was used and plotted as function of radius and depth only (Figure 5-1).

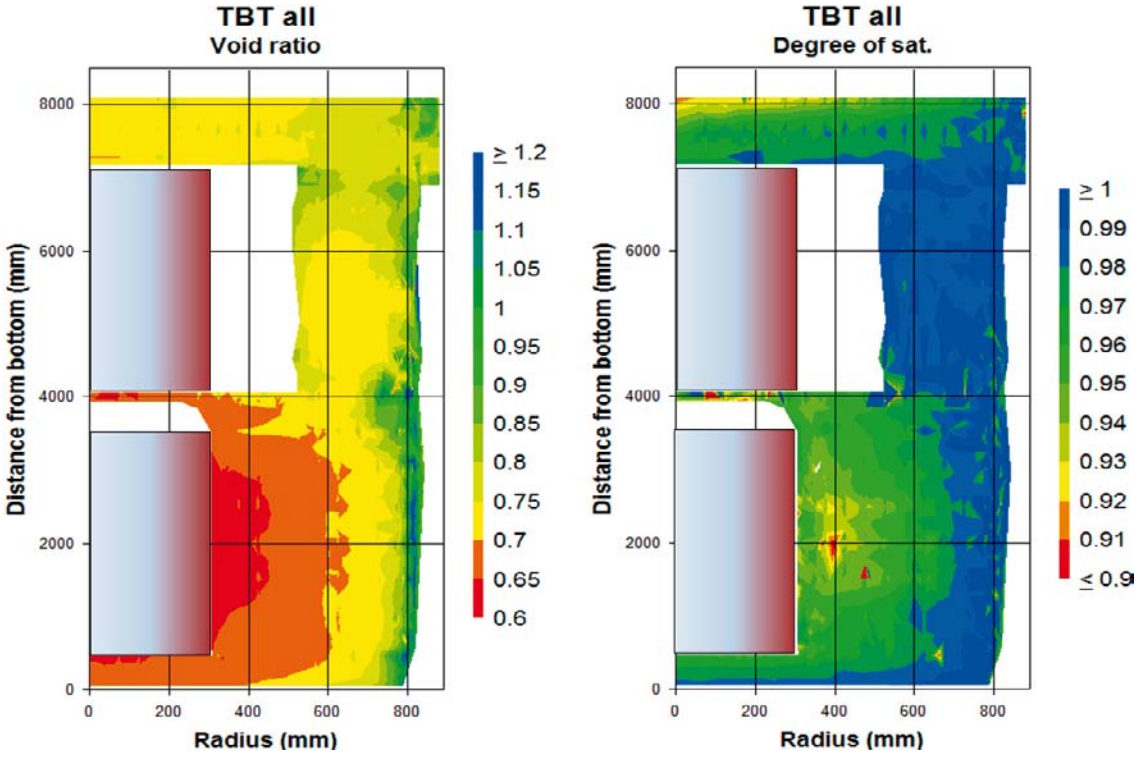

Figure 5-1. *Results from measurements of density and water content. Distributions of void ratio (left) and degree of saturation (right) at the end of the test.*

6 Hydro-mechanical and chemical characterizations

6.1 General

The main goal of the hydro-mechanical and chemical/mineralogical characterization program was to investigate if any significant differences could be observed between samples taken from the TBT field conditions with high temperature and high thermal gradient on one hand, and reference material on the other. This characterization program was described in detail by Åkesson et al. (2012a). The summary presented below is primarily based on this report, which therefore is not mentioned in the text any further.

The plan for the analyses was to first perform a primary scan on field test samples taken at 10 cm intervals from the mid-section of the lower heater (Figure 6-1). The characterization program focused on this section since it exhibited the most adverse thermal conditions in the experiment. Several analyses were performed on all field test samples, whereas other resource-demanding analyses were limited to samples taken from the inner parts of this section. All analyses were performed on reference material. A secondary scan was subsequently defined based on the outcome of the primary scan. The motive for these additional analyses mainly concerned the possibility to make indications of changes statistically significant.

The main part of the analyses was performed on samples obtained from the big sector from the 32° direction in Ring 4. The reason for selecting this particular big sector was that it was comparably intact after dismantling and that it did not contain any instruments.

The main part of the chemical/mineralogical analyses was performed on samples obtained by sawing pieces from the top level of the big sector. Each sample represented a radial width of 2 cm and was made large enough to supply material from the specific position for several of the planned tests. A sample representing the bentonite surface towards the heater was obtained by scraping 1–2 mm from the big sector specimen (radial position 30 in Figure 6-1). Several analyses were performed on bulk samples, as well as on Na converted fine fractions (<0.5 µm).

The main part of the hydro-mechanical analyses was performed on samples obtained by core drilling in the big sector. The radial positions of these cores largely corresponded with the positions of the sawed samples.

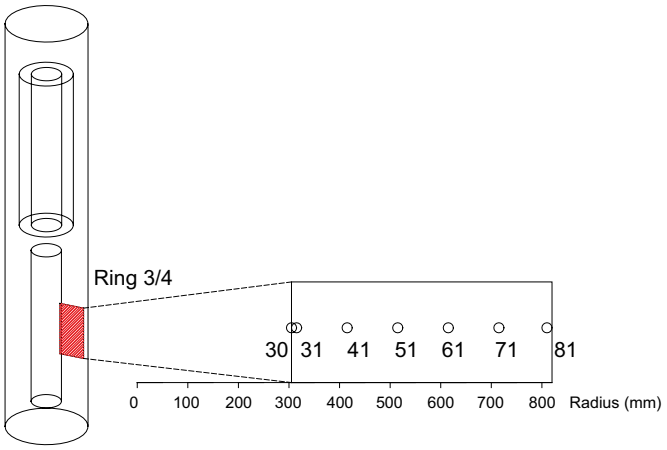

Figure 6-1. *Specified radial sample positions for the main part of the analyzed samples.*

6.2 Hydro-mechanical analyses

Retention curves

Water retention curves, i.e. the relation between the relative humidity and the water content, were measured for one field test sample (taken at 31 cm radius), as well as reference material. Both bulk material and Na converted fine fraction were analyzed. Each sample was exposed to eight different relative humidities.

The results from the bulk materials, both reference material and material from the field experiment, coincided well with previous results on bulk material of MX-80. However, the water content of the field test sample was slightly lower at a relative humidity of 97%. Measurements on samples with Na converted fine fraction showed no large difference between the reference material and the field test sample.

Measurements of swelling pressure and hydraulic conductivity

Measurements of swelling pressure and hydraulic conductivity were performed on field test samples taken from basically all specified radial sample positions, and on reference material. Field test samples were either trimmed or air-dried, ground and re-compacted (#1 series). Reference material was either directly compacted to different dry density values (#1 series); or prepared in ways similar to the field test samples, or subjected to drying (#2 series).

The field test samples showed a reduced swelling pressure, especially for the innermost samples (Figure 6-2, left). These samples also displayed a scatter in hydraulic conductivity, but with a tendency towards increased values on ground and re-compacted samples, and on trimmed samples from the innermost part.

The reference material (see Figure 6-2, right), showed that the swelling pressure displayed a scatter of approximately 10%. No large deviation was found between directly compacted, drilled, or ground and re-compacted samples. However, a trend of decreased swelling pressure was found for dried material. The reference material also showed that the hydraulic conductivity displayed a scatter of approximately 30%. No deviation was found between samples prepared by direct compaction, and those prepared by drilling. However, a trend of increased hydraulic conductivity was found for ground and re-compacted samples, as well as for dried material.

Triax

Two triaxial tests were performed; one with field test material (taken at 37 cm radius) and one with reference material. The stiffness as well as the deviator stress at failure was larger in the field test material than in the reference material, whereas the strain at failure was lower (Figure 6-3). The differences may be an effect of the decrease in swelling pressure observed at the innermost sample positions (see Figure 6-2), since the effective mean stress was approximately the same in the two triaxial tests, although the dry density was higher in the field test sample (1,660 kg/m^3) than in the reference sample (1,625 kg/m^3).

Uniaxial compression test

Uniaxial compression tests were performed on field test samples taken from basically all specified radial sample positions, and on reference materials. Three different sample types were tested: short (2 cm high) re-saturated samples, tall (4 cm high) re-saturated samples and short samples without re-saturation.

The tests showed that the strain at failure was reduced in all field test samples. Reference materials which were exposed to 120°C during 24 hours did also exhibit a reduction in the strain at failure.

The maximum deviator stress was basically unaffected with the exception for field test samples from the innermost position. Samples without re-saturation from the same radial position did not show any decrease in maximum deviator stress. This could possibly be an effect of more intact samples being used for the direct shearing tests.

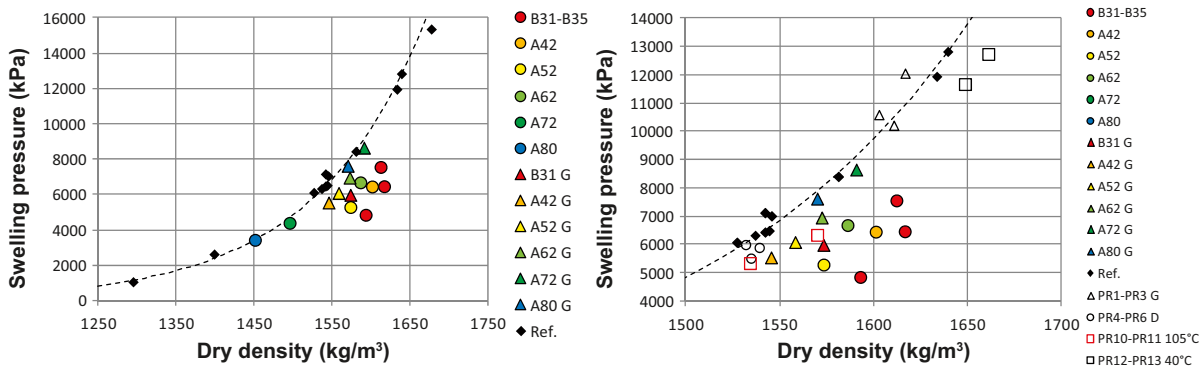

Figure 6-2. *Swelling pressure as a function of dry density. Field samples are denoted with colored markers: red to blue are used for the warmest to the coldest radial sample position (indicated by the labels); circles and triangles denote trimmed, and ground and re-compacted samples, respectively. References samples are denoted with black (test series #1) or unfilled markers (test series #2).*

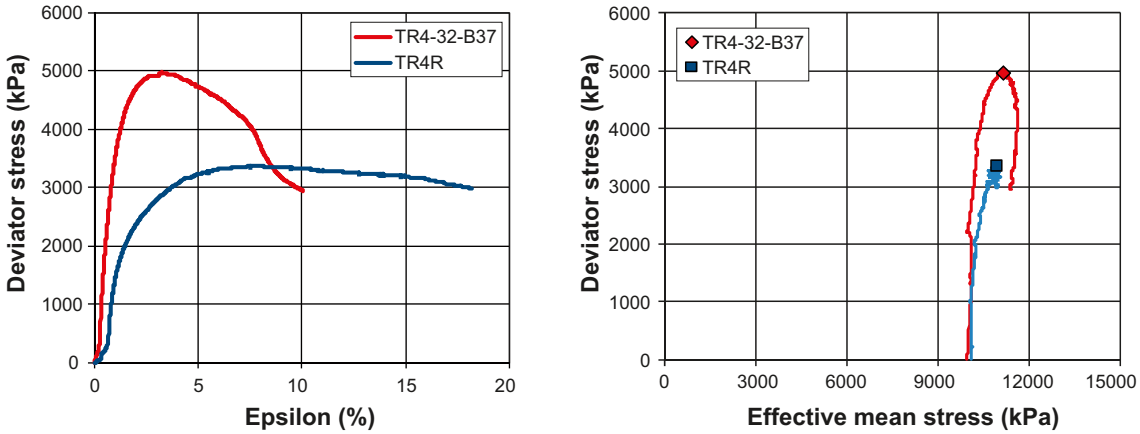

Figure 6-3. *Deviator stress versus strain in the triaxial tests (left). Stress paths plotted as deviator stress versus mean effective stress (right).*

6.3 Chemical/mineralogical analyses

Aqueous leachates

Analyses of aqueous leachates were performed on bulk samples from all specified radial sample positions as well as reference material.

The concentration of chloride had increased in the entire block but the distribution was irregular with peak values at 61 and 81 cm. This was probably a consequence of the artificial saturation with groundwater, and the subsequent use of deionized water for the saturation. The peripheral maximum was associated with a rather abrupt increase in the water content of the bentonite.

A loss in sulfate in the proximity of the hydration source and an increase in the inner part of block Ring 4 suggest that calcium sulfate, which has temperature dependent solubility, had been re-distributed along the gradients in temperature and hydration that prevailed during the test period.

The analyses of inorganic carbon displayed a tendency of decreasing levels towards the heater.

Cation exchange capacity (CEC)

Analyses of CEC were performed on bulk samples and Na converted fine fractions from all specified radial sample positions as well as reference material.

A tendency of increasing CEC towards the heater were observed in both data sets (see Figure 6-4 left) but the changes relative the references were close to the resolution of the method. Furthermore, changes in CEC may result as a net effect of the various dissolution/precipitation reactions that have occurred in the proximity of the steel heater.

Exchangeable cations (EC)

Analyses of EC were performed on bulk samples from all specified radial sample positions as well as reference material.

The relative proportion of the extracted cations in the reference samples was: 68% sodium, 22% calcium, 8% magnesium and 2% potassium. In the innermost part of the block, the proportion of calcium has increased at the expense of sodium mainly, suggesting some exchange of sodium for calcium. Such exchange would be an expected effect of the dissolution of Ca-carbonate, which would change the exchangeable cation pool (see Figure 6-4 right). Sodium was, however, the predominant cation in all samples also after the field test.

In general, the sum of cations exceeded the CEC by a few units, but sample A61 was exceptional in this respect, having a cation sum exceeding CEC by 13 meq/100 g. Thus, the contribution from soluble salts seemed to be significant in this sample and most of the cations displayed a more or less pronounced maximum at this position in the block.

Chemical composition of the bentonite

Analyses of the element content (ICP/AES+MS,EGA) were performed on bulk samples and Na converted fine fractions from all specified radial sample positions as well as reference material.

The acid-soluble carbon displayed a clear trend of decreasing values from the middle of the block towards the heater, whereas the content of the acid-insoluble carbon varied insignificantly along the different sample positions. This suggested that carbonates were dissolved in the warmest part during the field test.

The distribution of total sulfur was consistent with the results of the aqueous leachates, which indicated sulfate depletion in the peripheral part and accumulation in the middle part of the block.

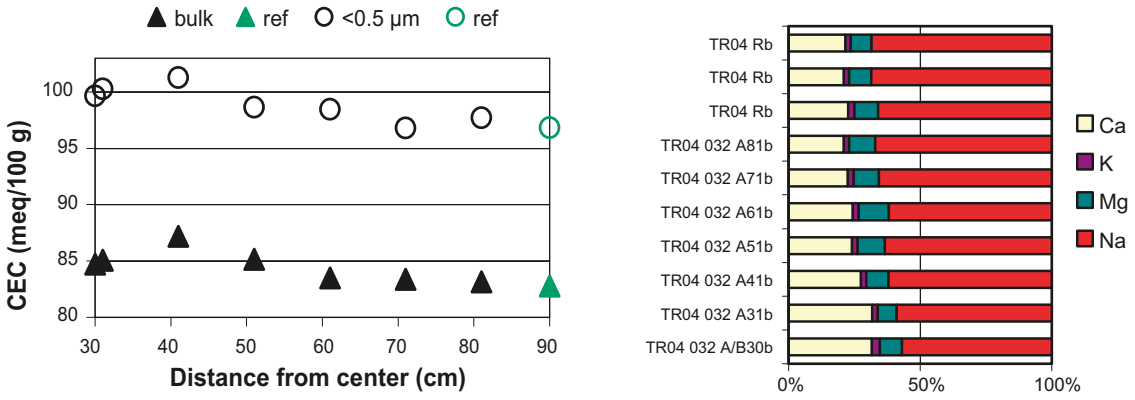

Figure 6-4. *Mean CEC values of the bulk samples and of the < 0.5 µm fractions (left; data for references are plotted at 90 cm). Relative proportions of the cations extracted by exchange against NH_4 in alcoholic solution (right).*

Corrosion of the steel heater resulted in contamination of the inner block surface by iron, which had increased from 3.66% Fe_2O_3 (mean of three reference samples) to 7.49% Fe_2O_3 in sample A30 (Figure 6-5 left). The corrosion products occured as stains on the block surface, but it was clear that iron also has been incorporated into the bentonite matrix in sample A31. The excess iron of the innermost samples was insignificantly reduced by the fractionation used for purification of the smectite, but most of the excess (90–95%) dissolved in a citrate-bicarbonate-dithionite solution, which more or less selectively extracts "free" iron oxides (e.g. hematite, magnetite) and oxyhydroxides (e.g. goethite).

The magnesium distribution also displayed a gradient with a distinct maximum at the heater, where the MgO content of the bulk bentonite had increased from 2.49% to 4.47% (Figure 6-5 right). The outer part of the block was slightly depleted in magnesium, suggesting an inward transfer of magnesium along the thermal gradient. All fine clay fractions of the field test samples had gained some magnesium compared to the reference, although the increase in sample A30c was outstanding. Less than 15% of the excess magnesium in sample A30c was extracted into the CBD-solution, and this fact, together with the facts that the fine clay was Na-converted and carbonate-free, suggests that the major fraction of the magnesium excess exists in a non-exchangeable, insoluble form.

Smectite composition

The chemical composition of the Na-converted <0.5 µm fractions has been used for calculations of the average structural formula of the smectite. The calculation was based on the structures of 2:1 layer silicate, assuming an anionic charge of –44, in addition to the following assumptions and simplifications: The iron content was corrected for CBD-extractable iron. The remaining iron was allocated to the octahedral sheet of the smectite and assumed to be trivalent. Potassium (0.02–0.03% K_2O) in the Na-converted clay was considered non-exchangeable and was allocated to illite. Any calcium that may exist after the dialysis of the Na-converted clay (0.01–0.04% CaO) was assigned to the pool of interlayer cations. Magnesium, corrected for the CBD-extractable fraction, was assigned to the octahedral sheet. Silica was corrected for the small amounts extracted by the CBD-treatment and the rest was allocated to the tetrahedral sheet of the smectite.

The calculated average structural formulae of the smectite of field test and reference samples are given in Table 6-1. The structural formulae of the reference samples are almost identical ($(Al_{3.16}Mg_{0.45}Fe^{3+}_{0.34})\ (Si_{7.87}\ Al_{0.13})\ O_{20}(OH)_4\ X_{0.70}$ where X is a monovalent interlayer cation) and typical of montmorillonite, in which the charge arises mainly from divalent cations in octahedral sites. The smectite structure of most of the field test samples deviated insignificantly from that of the reference samples, sample A30c being the most conspicuous exception. The formula of the latter sample suggests a major redistribution of the charge between the tetrahedral and octahedral sheets, as an effect of a significant substitution of octahedral Al by Mg, and a corresponding substitution of tetrahedral Si by Al.

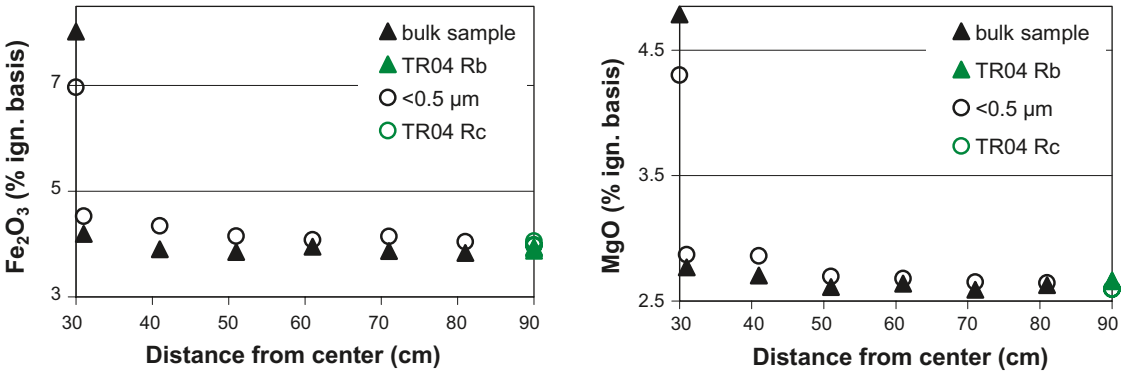

Figure 6-5. *The distribution of iron (left) and magnesium (right) in bulk samples and in Na-saturated fine clay fractions. Concentrations in weight % on an ignited basis. The reference samples are plotted at the position 90 cm.*

Table 6-1. Calculated mean structural formula of the purified smectite fraction. The calculations are based on the chemical composition of the Na-saturated <0.5µm fraction corrected for CBD-extractable elements. The result for sample A30c (in red) is discussed in the text.

	TR04 032 with correction for CBD-extractable Fe, Si, Mg									
	Rc-1	**Rc-2**	**Rc-3**	**A30c**	**A31c**	**A41c**	**A51c**	**A61c**	**A71c**	**A81c**
Si	7.86	7.87	7.88	7.72	7.83	7.81	7.84	7.84	7.86	7.87
Al	0.14	0.13	0.12	0.28	0.17	0.19	0.16	0.16	0.14	0.13
Σ tet	8.00	8.00	8.00	8.00	8.00	8.00	8.00	8.00	8.00	8.00
Al okt	3.15	3.16	3.15	2.94	3.11	3.12	3.15	3.15	3.15	3.14
Ti	0.01	0.01	0.01	0.01	0.01	0.01	0.01	0.01	0.01	0.01
Fe^{3+}	0.34	0.34	0.34	0.41	0.36	0.36	0.34	0.34	0.35	0.34
Mg	0.45	0.45	0.45	0.74	0.50	0.49	0.46	0.46	0.46	0.46
Σ oct	3.96	3.96	3.95	4.10	3.98	3.98	3.97	3.97	3.97	3.95
Ca	0.003	0.003	0.003	0.006	0.001	0.004	0.005	0.001	0.004	0.003
Na	0.71	0.70	0.70	0.71	0.73	0.72	0.69	0.70	0.69	0.72
interlayer charge	0.71	0.70	0.70	0.72	0.73	0.72	0.70	0.70	0.70	0.72
% tet. Charge	20	19	17	39	24	26	23	22	21	17
molar weight	745	744	744	749	746	746	745	745	744	744
CEC calc.	96	94	94	96	98	97	94	95	94	96

To validate the results of the formula calculation, the CEC of the <0.5 µm fractions was determined after the clay had been saturated with Li and heated at 250°C (Greene-Kelly test). The remnant CEC of the samples after Li-saturation and heating should represent the tetrahedral charge of the smectite. The CEC of the heated Li-clays was however more or less constant. Consequently, the charge distribution, determined by CEC measurements before and after Greene-Kelly treatment, and by formula calculations based on chemical composition, respectively, displayed a clear discrepancy for the magnesium-rich sample A30c. It remains to establish whether the allocation of all non-exchangeable magnesium to octahedral sites in smectite has a true structural foundation, or whether the sink of magnesium is a neoformed phase.

Mineralogical composition

X-ray diffraction (XRD) analyses were performed on bulk material from all specified radial sample positions and on reference material. The diffraction pattern of random powders of the bulk samples are presented in Figure 6-6, where the strongest peaks of the major non-phyllosilicates gypsum, quartz, cristobalite, plagioclase, anhydrite and calcite are indicated together with the (001) and (003) basal reflections and the hk reflections of montmorillonite.

The XRD patterns of the random powders were used for quantitative evaluations by use of the Siroquant software, in which the montmorillonite (02,11) and (13,20) reflections indicated as (mm, hk) in Figure 6-6 were used to evaluate the montmorillonite content. The results of the quantitative evaluations of the main identified mineral phases are presented in Figure 6-7. Three obvious tendencies are revealed in the quantitative data, one being the change of the calcium sulphate phase from gypsum to anhydrite in the warmer inner part of the bentonite, one being the loss of calcium carbonate (calcite) in the inner part of the bentonite, and one being a marked decrease of cristobalite in the bentonite in close proximity to the iron heater.

The d-value of the (060) peak was more or less identical in all samples (~1.50 Å), and provided no obvious evidence of a change in the *b* cell dimension of the clay mineral, which would be an expected effect of a change of the amount of Al in tetrahedral coordination, as was indicated in the structural formula of sample A30.

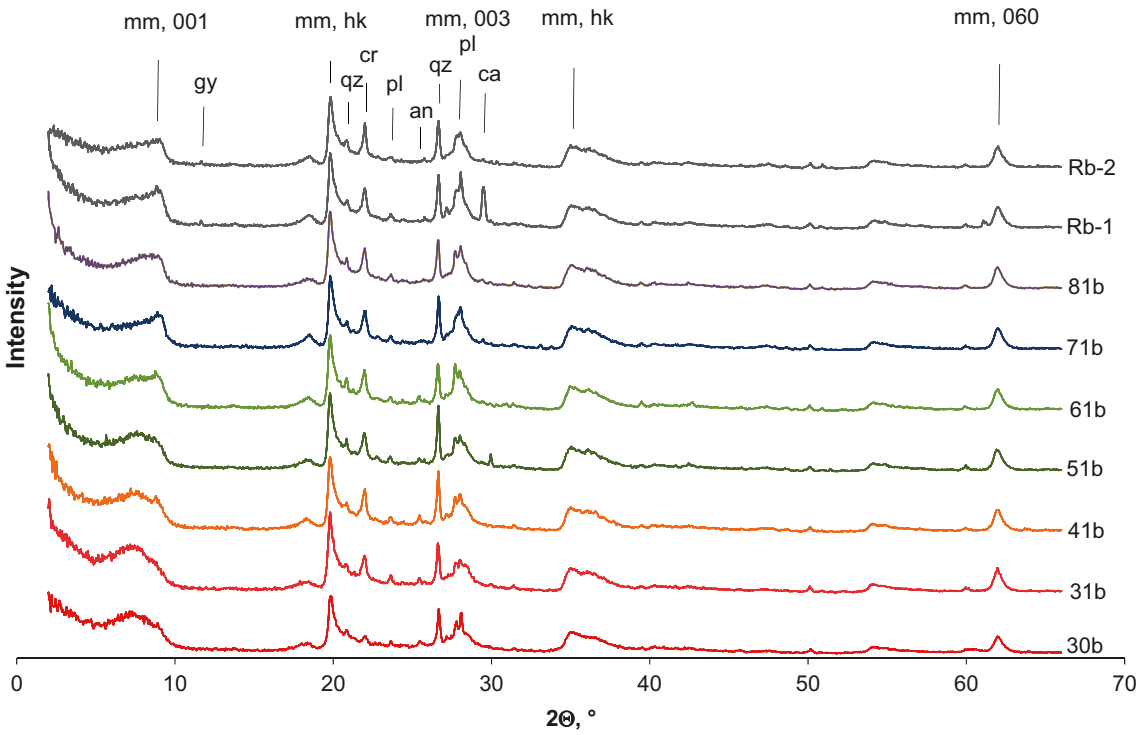

Figure 6-6. *XRD profiles of all analysed bulk samples. Sample positions and references are indicated to the right. an = anhydrite; ca = calcite; cr = cristobalite; gy = gypsum; pl = plagioclase; qz = quartz; mm = montmotillonite. Random powders. CuKα radiation.*

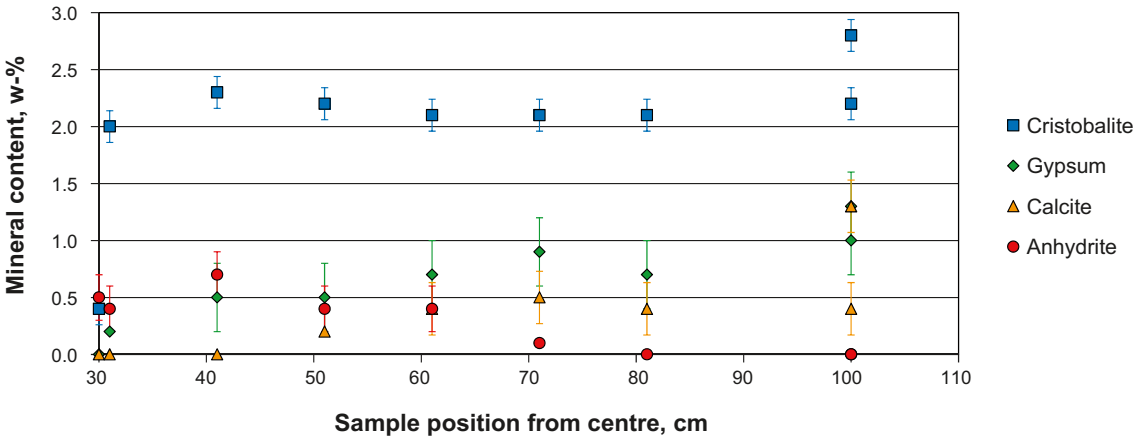

Figure 6-7. *Content of cristobalite, gypsum, calcite and anhydrite versus radial distance in the analysed section. Results for the reference samples Rb-1 and Rb-2 are shown at the fictive distance 100 cm.*

XRD-profiles of oriented mounts of the Mg-saturated, air-dried and EG-solvated <0.5 µm fraction of the two innermost samples showed that the fine clay fractions appeared to be montmorillonite with the exception of traces of cristobalite. No difference was seen in the expansion behaviour of the clays, which all expanded to approximately 16.9 Å upon EG-solvation.

In summary, the available XRD data provided no clear evidence of any structural changes in the montmorillonite.

Transmission electron microscopy (TEM)

Analyses of isolated particles from the fine fractions (<0.5µm) were made on reference and Fe/bentonite interface material (radial position of 30 in Figure 6-1). No significant morphological differences were found. Typical montmorillonite structures dominated both materials, but more grain-like structures were occasionally found.

Most analyses showed element compositions typical for montmorillonite, but the grain-like structures had a significantly increased Si/Al ratio. Seven spectra were obtained for the field test sample. Three spectra represented typical montmorillonite structures and included all relevant elements, and were therefore used for calculating the structural formulas. Using the Na^+ value which gives the measured CEC and the mean value of the three spectra, the following mean structural formula was calculated for the A30c montmorillonite structure:

$$Si_{7.75}\ Al_{0.25}\ Al_{2.88}\ Fe\ (III)_{0.46}\ Mg_{0.76}\ Ca_{0.02}\ K_{0.03}\ Na_{0.65}$$

The result may thereby be compared with the ICP/AES results for the A30c sample in Table 6-1 which in principle include the same type of information.

Scanning electron microscopy (SEM)

A SEM/EDX element analysis was performed on a beam shaped sample, approximately 15 cm long, taken from an inner piece adjacent to the heater surface in Ring 4.

The field test bentonite was studied radially from the steel/bentonite interface and outwards with respect to visible precipitates and element distribution. The general picture was that no significant morphological differences were found along the studied sample. The only exception was distinct iron-rich clusters which were found in the proximity of the steel/bentonite interface. The size of the individual clusters was less than 50 µm. In order to minimize the scatter and study the general trends, area analyses (A = 250 µm × 250 µm) were performed at increasing distances from the iron/bentonite interface. The results showed the typical element distribution for MX-80 bentonite, but with significantly higher content of iron and magnesium in the innermost centimetres (Figure 6-8).

SEM/EDX element analyses of the heater surface material were used to check if the steel itself, or remnants from blast sand, could be the source of the accumulated magnesium found in the inner part of the bentonite. No indications of blast sand were however found, and the Mg content in the steel alloy was insignificant. There was consequently no indication that the heater was the origin of the accumulated magnesium.

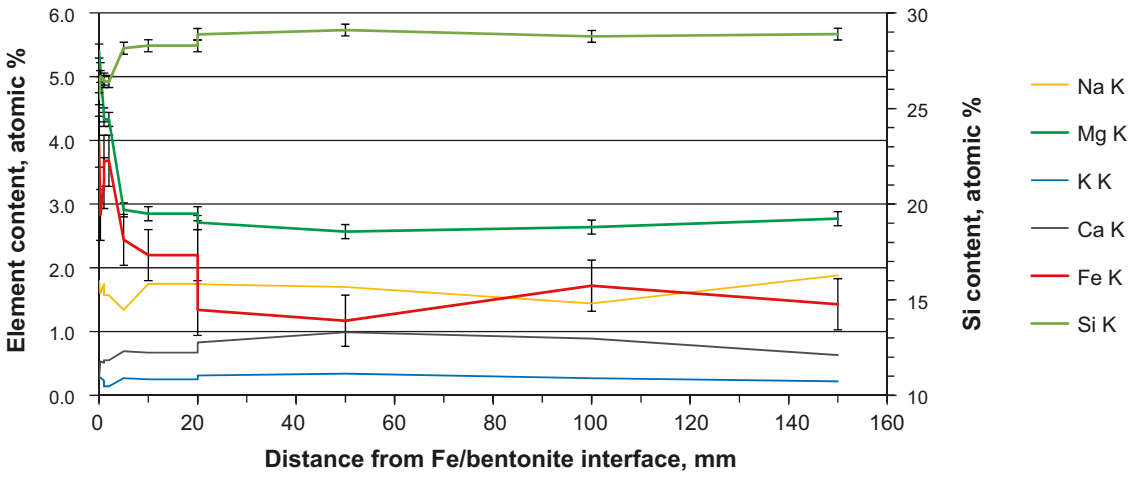

Figure 6-8. *Mean results from SEM/EDX areas analyses (A = 250×250 µm²) plotted against the distance from the iron/bentonite interface to the area midpoint. Error bars indicate ± 1 stdv based on 5 analyses in the outer part of the bentonite.*

Mössbauer spectroscopy

Six samples (four field test samples from Ring 3, taken at 10, 30, 50 and 90 mm from the heater surface, denoted C31, C33, C35 and C39, respectively, below; and two reference samples) were studied with Mössbauer spectroscopy. The first spectra were collected at 77 K in transmission mode using a sinusoidal velocity scale with a maximum Doppler velocity of 10.1 mm/s. These spectra were fitted utilizing spectral components corresponding to four paramagnetic doublets (component 1, 2, 3 and 5) and one magnetic sextet (component 4). For the paramagnetic components, fit parameters were quadrupole splitting, isomer shift and spectral intensities. For the magnetic component, the internal field and its gaussian distribution were included as fit parameters as well. All components were constrained to have a common line width. Components 1 and 5 had large isomer shift, which is typical of divalent Fe. Components 2 and 3 can be attributed to trivalent Fe, based on their low isomer-shift values.

The main result of the analyses, i.e., the ratio of paramagnetic Fe^{2+} to Fe^{3+}, was obtained from the spectral intensity values. Assuming the recoil-free fraction to be the same for all components, the valence ratio is the intensity of components 1+5 to that of components 2+3. The variation in the intensities of different components in the two reference samples was however of the same magnitude as the variation in the intensities of the field test samples. The ratio of Fe^{2+} and Fe^{3+} has therefore not changed significantly. Hence, the increase in the amount of iron was probably too small to be detected reliably with Mössbauer spectroscopy.

An alternative fit, including only three spectral components, was also prepared. Component 1 and 2 were assigned to Fe^{2+} and Fe^{3+}, respectively, in clay minerals, whereas component 3 (magnetic) was assigned to some accessory mineral(s) in the sample. The intensity of component 1 has increased slightly in samples C31, C33 and C35 compared to reference samples and sample C39, which indicates that the amount of Fe^{2+} has increased slightly in the samples.

A second round of spectra was collected at a maximum Doppler velocity of 4.59 mm/s for two of the samples: the C33 sample and the reference material. The ratio of the paramagnetic Fe^{2+} and Fe^{3+} components was slightly higher in the field test sample than in the reference sample.

Fourier transform infrared spectroscopy (FTIR)

FTIR analyses were performed on bulk samples from all specified radial sample positions as well as reference material. In addition, analyses of Na converted fine fraction from radial position 31 (Figure 6-1) and reference material were performed.

Analyzed field test samples showed a decrease in cristobalite (and/or opaline silica) content towards the heater. Additionally, potential decrease in calcite content, towards the heater was found. Also potential decrease in intensity of AlAlOH deformation band of smectite was seen in the A30 sample. No indications for change in band intensities or positions that can be assigned to calcium sulphates were found.

The differences between the Na converted fine fractions for the reference samples and the A31c sample were minor. Only small decrease in the intensity of silica band at 798 cm^{-1} was seen.

7 THM modelling

7.1 Introduction

Several modelling tasks have been carried out since the beginning of the TBT project: from the initial scoping calculations, the predictions and the first evaluations of the field test, over the predictions and the evaluations of the two parallel mock-up tests, to the final modelling task of the field test after the dismantling of the field test. This chapter summarizes these modelling tasks in general and the final task in particular.

7.2 Scoping calculations

Hökmark et al. (2005) described three preliminary studies initiated prior to finalizing the test design. These studies were scoping calculations conducted in order to explore the general feasibility of the test, to find out what the power requirements would be to achieve the test objectives, and to get a first estimate of the time-scale of the water uptake process.

Study 1 was a simplistic thermal study performed to find the power required to achieve the objectives of the test. The study was based on analytical solutions of the temperature field around a line heat source and on steady-state expressions for the temperature distribution between two cylindrical surfaces, i.e. the heater surface and the wall of the deposition hole. The heater package was represented by a line heat source. The analytical line source solution was used to calculate the temperature at the wall of the deposition hole as a function of time, and the steady-state expression to find the temperatures in the annular space between heater and rock. Both barrier configurations were analyzed.

Study 2 was a numerical quasi 3-D thermal calculation of the temperature field around the TBT heater package. The calculations were performed using the finite element code ABAQUS. There was one main set of calculations and one supplementary set with different (or modified) assumptions regarding the geometry and the distribution of the heat power.

Study 3 regarded numerical 1-D radial symmetry Hydro-Thermal calculations of the water uptake process. The calculations were performed with the CODE_BRIGHT program. There were two model geometries: one for the composite sand-bentonite barrier and one for the single material barrier. The thermal input to the finite element models was based on the results of Study 1.

7.3 Predictions

Hökmark (2005) and Hökmark et al. (2007) described the predictive modelling phase which was initiated in late 2002, and was completed by late May 2003. For the predictive modelling phase, a program was issued in November 2002. The program specified the geological environment, the heat transport properties of the TBT tunnel rock mass, the geometry of the experiment, the material properties and the thermal load conditions. Predictions of a number of variables (temperature, saturation, pressure, RH, etc) were asked for at a number of points and on a number of vertical and horizontal scanlines, although it was left to the participating teams to decide upon the level of effort and to decide upon the necessary idealizations and simplifications. Predictions were asked for a number of times after the test start up to 1,200 days. A number of modelling groups gave predictions of the THM evolution at the points and scan-lines described in the predictive modelling program. These were:

- EDF team, organized by ANDRA, using Code_Aster.
- EuroGeomat team, organized by ANDRA, using code Cleo.
- UPC/DM Iberia team, organized by ENRESA, using CODE_BRIGHT.
- Clay Technology team, organized by SKB, using ABAQUS and CODE_BRIGHT.

All simulations (except for the ClayTech CODE_BRIGHT simulations, see Fälth et al. 2005) were performed with 2D axisymmetric model geometries, which included the deposition hole as well as a substantial portion of the surrounding rock.

Some of the models did predict formation of a stable saturation front around the lower heater. This was the case for both CODE_BRIGHT models, where no signs of resaturation of the hottest parts were found within the simulated time range. For the ClayTech model this was probably caused by the specified atmospheric gas pressure. The ABAQUS model did, however, predict some resaturation to have occurred after 750 days. All these models, in particular the two CODE_BRIGHT models, overpredicted the extent and scope of drying.

The sand-shield, around the upper heater, was not explicitly represented in the UPC/DM CODE_BRIGHT model and in the ABAQUS model which both predicted some desaturation of the nearby bentonite while the other models did not. In the ClayTech CODE_BRIGHT model, desaturation was prevented by vapour moving in from the sand-shield which was assumed to contain a small amount of liquid water at the time of emplacement.

7.4 Evaluation modelling

Åkesson (2006a) presented two issues that were addressed within the evaluation modelling task framework during 2004.

Step I

Step I addressed the possible effects of a 750 W power increase of the upper heater. A modelling program was distributed in March 2004. Contributions were presented in May 2004 from UPC and ClayTech. Calculations were made for two different schemes of overheating for the upper heater. In both cases, the overheating was supposed to start at day 433 (June 2004) from 1,500 W, and increasing thereafter up to 2,250 W. In the slow case, the increase was made during a period of 30 days, whereas in the rapid case, the increase was made in 6 days. Both UPC and ClayTech used CODE_BRIGHT and large quasi-3D thermo-hydraulic models for the problem. These models displayed many similarities, although they were quite different regarding the temperature levels in the sand shield. Still, both models suggested that the overheating scheme would have a low impact on the saturation process and it was therefore decided to abandon the overheating activity.

Step II

Step II addressed the hydro-mechanical developments around the upper heater, and aimed at explaining the unexpected HM-trends, with temporarily increasing suction values and decreasing stresses, observed in this part (see section 3.4). A modelling program was distributed in August 2004, and model contributions were presented by teams from UPC and ClayTech, both using CODE_BRIGHT for their work. The geometry of the UPC model was identical to the model used in Step I. ClayTech, on the other hand, used smaller geometries covering only a 1D axisymmetric section around upper heater. UPC presented results for three cases, all fully coupled THM models. ClayTech presented results for seven models, both HM and TH models, but no fully coupled THM model. The models from both teams captured the general trends well, especially the UPC models, and implied that the temporary stress/suction trends was a consequence of an limited supply of water. The results did not lend support to the alternative explanation that the disturbance was caused by a mechanical phenomenon. A failure could for instance lead to an unloading, which would influence the suction value at constant water content.

TBT_2

Åkesson (2006b) presented the predictive modelling of a mock-up test (TBT_2), which was planned, designed and carried out by CAE in Saclay (France), addressing the desaturation process observed in the field test around the lower heater. The mock-up test was performed on a compacted cylindrical specimen of MX-80 bentonite 200 mm in height and diameter. The thermal loading was divided in

three phases: a nominal, an optional and a transient phase. In the nominal phase, a thermal gradient was gradually increased from zero to a maximum of 1.8°C/cm. The protocol for the optional phase aimed at establishing a 3°C/cm gradient in the sample, then at elevating temperature keeping the thermal gradient constant.

A modelling program for the specified task was issued in April 2005, and model predictions were presented by teams from UPC and ClayTech, both using CODE_BRIGHT for their work. The problem was further elucidated with the use of an analytical solution of steady-state conditions, i.e. a state at which the suction driven advective flow equals the diffusive vapor flow in all points. All predictions and test results showed that moisture redistribution takes place as soon as there are thermal gradients. The results therefore do not support the notion of thermal threshold gradients. As far as long-term effects are concerned, the difference in temperature between the hot and cold ends, rather than the gradient determines the extent of desaturation at the hot end. This is a consequence of the applied conceptual models and was demonstrated both by use of FEM codes and by use of an independent analytical solution.

TBT_3

During the course of the work with TBT_2 it was found that the experiment suffered from a thermal leakage. A new mock-up experiment, TBT_3, was therefore defined. Measures were taken to avoid the thermal leakage in this experiment. The test was more instrumented than previously, while the applied thermal protocol was simpler. This protocol was divided in three phases: (i) an initial homogenous thermal ramping during 15 days from room temperature at 22°C up to 84°C, (ii) a temperature increase at the hot face during 15 days up to 120°C, with cold face temperature constant at 84°C, and (iii) an equilibration phase with constant thermal gradient. The latter phase was allowed to continue for 72 days.

Åkesson (2008) described the predictive modelling of TBT_3. A modelling program for the specified task was issued in March 2006. This program prescribed a total duration of the test of 50 days. Model predictions were presented by teams from UPC and ClayTech, both using CODE_BRIGHT for their work.

A comparison of experimental relative humidity data with predictions revealed three significant deviations: i) the relative humidity at different sensor position clearly separated during the initial phase, ii) the relative humidity at the cold end increased to 100%, and iii) steady-state conditions were not reached within 50 days. Whereas the first deviation appears to have been caused by the minor temperature gradient during the initial phase, the second and the third deviation appears to be real physical phenomenon that were not captured by the models.

The predictions of the final profile of the degree of saturation were not comparable with the experimental results since the test was terminated and dismantled at a much later date than in the predictions. Nevertheless it was interesting to notice that both models predicted a higher redistribution, with more extreme end-point values, than was found in the experiment.

Åkesson (2008) and Åkesson et al. (2009) described the evaluation modelling of TBT_3. This was performed after the experiment was completed (after 102 days) and the modelling teams therefore had access to the experimental results. The contribution by the UPC team focused on improving the hydro-mechanical processes while the ClayTech team focused on the thermo-hydraulic processes.

The mechanical constitutive law used for the predictions was based on the Barcelona Basic Model (BBM). In order to improve the model with respect to the hydro-mechanical processes, another constitutive law was used, namely the Barcelona Expansive Model (BExM). Experimental values were compared with two simulations, one using the classical BBM model and the other one using the new Expansive model. It became evident that the Expansive Model was able to simulate both the expansion of the bentonite in the cooler zone and the compression at the hot side using a single set of parameters.

The evolution of vapor pressure and suction was evaluated from the experimental relative humidity and temperature data. The steady-state profiles showed that the suction gradient was significant, while the corresponding vapor pressure gradient was minor. This implied that the flow coefficient

for vapor transport was much higher than for liquid flow. Measured degrees of saturation and the steady-state suction values enabled an evaluation of a retention curve. The experimental results indicated that the bentonite can be unsaturated under these conditions, even though the vapor is saturated. The steady-state moisture distribution and the time to reach this state was analyzed with several axisymmetric 2D TH(g) CODE_BRIGHT models, for different vapor tortuosity factor values, and for cases with and without advective liquid flow. The separation of the relative humidity levels and the time-scale for this was fairly well captured by the models without advective flow, especially at the hot end and during the final phase. The agreement was however less good during the phase when the thermal gradient was increased, especially at the cold end. This could possibly be improved by modification of the function for the diffusion coefficient and the description of the retention properties.

7.5 Final THM modelling

Åkesson et al. (2012b) described the final TBT modelling effort, which was begun after the dismantling operation in 2010. The main part of this work was numerical modelling of the field test. Three different modelling teams presented several model cases for different geometries and different degree of process complexity. Two different numerical codes, CODE_BRIGHT and ABAQUS, were used. The work also included different evaluations of experimental results with the aim to validate a number of data sets, and to assess the conditions in the tests prior to the dismantling operation. Finally, the validity of the material models was assessed. This task was a test of the different parts, or constitutive equations, of the material models, especially for the bentonite, for their ability to reproduce the experimental data. The final THM modelling was completed during 2011.

UPC-Cimne contribution using CODE_BRIGHT

The modelling performed by UPC-Cimne, was divided in three subtasks.

In the first task, the response observed at the lower part of the in situ test was analysed. A reduced 2D-axisymmetric geometry was used, and a number of considerations were included in the analyses: (a) the use of the Barcelona Expansive Model for MX-80 bentonite; (b) updated parameters in the diffusive flow term to take into account the effect of high temperatures; (c) the use of a non-conventional water retention curve for MX-80 at high temperature. In general, the numerical simulations showed a good agreement with the measurements.

The objective of the second task was to find a possible relation between the cracks observed in the bentonite blocks at the upper part of the in situ test and the cycles of suction and stresses registered in that zone at the start of the experiment. A 2D-axisymmetric geometry which did not include the rock mass was considered in the analysis. Results confirmed that the cycles of suction and stress measured in the bentonite surrounding the upper heater was mainly due to a lack of water available for saturating the bentonite. Therefore the reason for that behaviour was mainly hydraulic. Measured values of thermal and hydraulic variables were in general well reproduced. The mechanical behavior of the bentonite blocks was simulated using the BBM. Parameters in this model were defined using experimental data from the literature. This set of parameters differed from those used in the simulations carried out in 2004 (section 7.4). However, it was not possible to reproduce the unexpected high deviatoric stresses registered at the start of the test at the mid-high of the upper heater.

The third task described the performance, observations and interpretation of the full-scale in situ heating test (TBT). Because convergence problems arose when changes in the boundary conditions were applied in the field test, it was not possible to carry out a full THM analysis until the end of the test. Therefore a model limited to the TH processes was analysed. The comparison between the results of the numerical analysis and the field observations suggests that the formulation and associated computer code are able to reproduce the main observed features of the THM behaviour of the test.

Clay Technology contribution using CODE_BRIGHT

The modelling performed by Clay Technology's CODE_BRIGHT team was divided into four sub-tasks, with the first three focusing on separate parts of the full geometry, and the fourth being a model of the full field experiment.

The first two modelling tasks were 1D axisymmetric models of the saturation process at mid-height of both heaters. Task 1 concerned the evolution around the lower heater, at the height of Ring 3 and 4. The model solved the thermal, hydraulic and mechanical problems. Due to the high temperatures in the bentonite (T>150°C) it was also necessary to solve the mass balance of air, including water vapour transport (see Figure 7-1). The conditions around the upper heater were modelled in task 2. The materials and boundary conditions were chosen so as to represent the evolution around mid height of the heater, at the location of Ring 9 and 10.

In the third modelling task an attempt was made to reproduce the shearing which appeared to have occurred in Cylinder 3. The evidence for this event comes from 1) a spike in the axial stress measured in Cylinder 3 at day 70, and 2) the displacements which were seen in Cylinder 3 during dismantling (see Figure 4-2 and 4-3). As this event occurred early on, the model was run for 200 days. It solved the hydraulic and mechanical problems only. The temperature during this period was approximately 60°C in the upper package in the field experiment, and for simplicity it was kept constant in the model at this value.

In the fourth modelling task, results from a 2D axisymmetric model of the full field experiment were presented. The model solved the Thermal and Hydraulic problem, as well as for the gas pressure. However, due to computational problems with such models, the mechanical problem was not solved. The motivation for this model was to understand how a lower gas pressure may influence the overall hydration in the experiment.

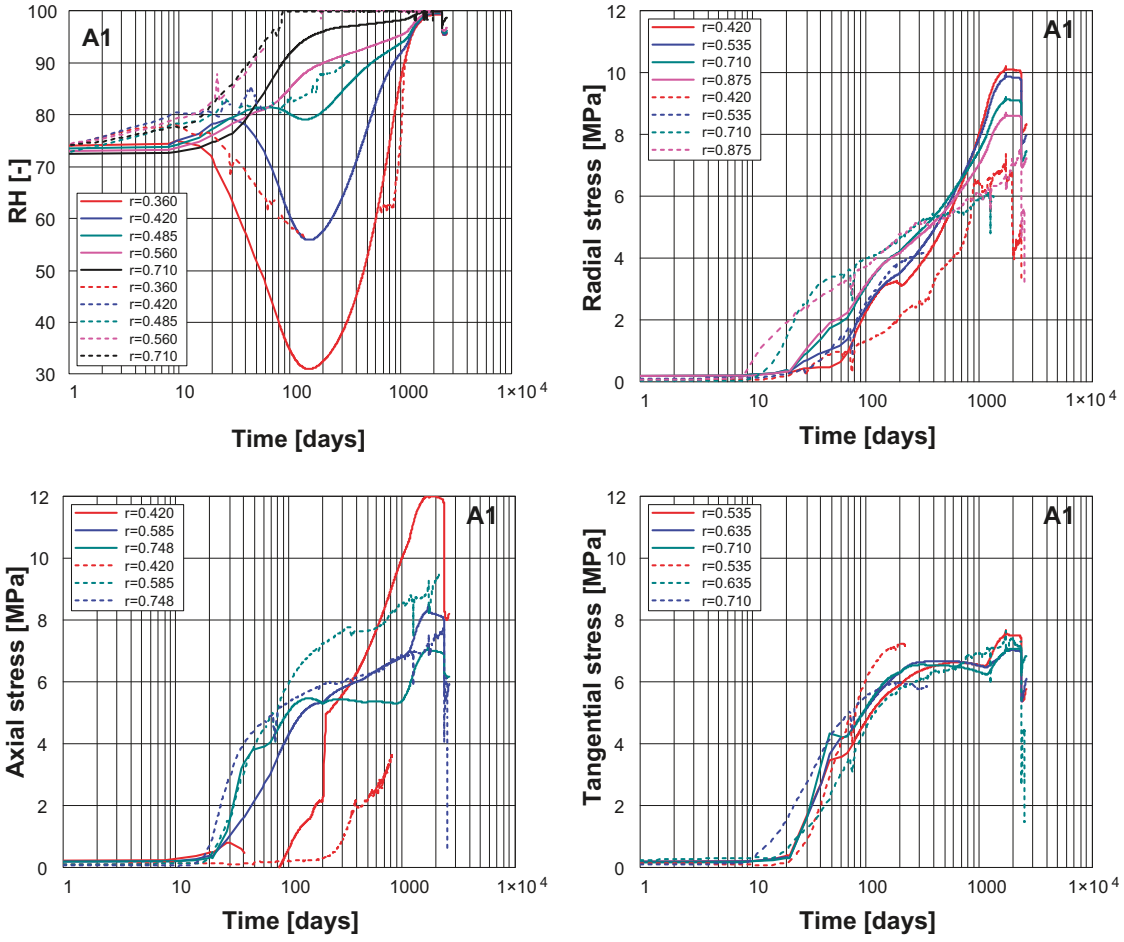

Figure 7-1. *Evolution of relative humidity as well as radial, axial and tangential stresses seen in one numeric THMg model (solid lines) compared with the actual evolution in Ring 3 and 4 (dashed lines).*

Clay Technology contribution using ABAQUS

The modelling performed by Clay Technology's ABAQUS team focused on a large-scale 2D axi-symmetric geometry which included the deposition hole as well as a substantial portion of the surrounding rock. The model solved the THM problem with a staggered solution technique facilitated by ABAQUS. The calculation was performed iterative so that the first loop of the temperature calculations were based on the thermal properties of the initial conditions of the buffer. The first loop of the hydro-mechanical calculations was subsequently performed using these temperature results. In the second loop of the temperature calculation the new thermal properties created by the hydro-mechanical evolution were used. Finally, the second loop of the hydro-mechanical calculation was based on the new temperature results. This implied however insurmountable problems which only could be solved by introducing damping forces and restarts.

The properties for the bentonite blocks were the same as previously used for the Canister Retrieval Test, although with a reduced value of the thermal vapor flow diffusivity.

In general the thermal results were adequate although the boundary conditions had not been fine tuned. The largest discrepancies were found for the lower heater. However, the thermal results were considered to be good enough for the HM-calculation. The hydro-mechanical modelling results were both good and bad, when compared with the experimental data. The evolution of the buffer wetting and buffer swelling pressure were quite well modelled. The agreement between modelled and measured force and displacement of the plug was also quite good. However, there were some parts of the void ratio distribution that were not well captured. The low void ratio level close to lower heater was not captured by the model. Neither was the very high void ratio measured in the outermost parts of the bentonite blocks captured by the model.

Evaluation of experimental data

The experimental results were evaluated with the aim to validate a number of data sets, and to assess the conditions in the tests prior to the dismantling operation. The evaluation was made in five different tasks:

i) The void ratio profiles measured during the dismantling were for 10 out of 16 blocks consistent with the dry density of the blocks after compaction (relative error $\leq 1\%$), if the initial block heights as well as the results from the leveling at installation and dismantling were considered.

ii) The void ratio profiles measured during the dismantling and the final total pressure readings were generally consistent with current swelling pressure curves (Figure 7-2). The final pressures in Ring 3, especially for the innermost sensor, were however slightly lower than swelling pressure curves.

iii) The results from this task indicated that the measured saturation profiles around Heater 1 could be caused by the thermal contraction of water if the bentonite was water saturated prior to the termination of the heating. Still, the possibility to reach the final saturation profile through an alternative route should not be excluded. This task also shed light on the high void ratio gradient observed close to the sand filter.

iv) The radial displacements in Ring 4 implied that the evaluated thermal conductivity values (see Goudarzi et al. 2010) were underestimated with approximately 4–8%.

v) Different experimental observations from the mid-section around the lower heater (saturation profiles; temperature profiles and evaluated thermal conductivities; pore-, filter- and saturated vapor pressures; total pressures; and relative humidity evolutions) have been identified as either supportive or refutable to: i) alternative hypothetical final states, before the termination of the heaters; and ii) different types of progress of saturation, with either smooth or broken profiles. The analysis was apparently non-conclusive, since all alternatives could be supported and in many cases refuted by the experimental data. Still, it appeared to be clear that the bentonite wasn´t totally water saturated during the final state. Moreover, the most plausible interpretation would be that the progress of saturation would be characterized by a broken saturation front, i.e. a saturation front in which the outer part was water saturated whereas the inner part was not.

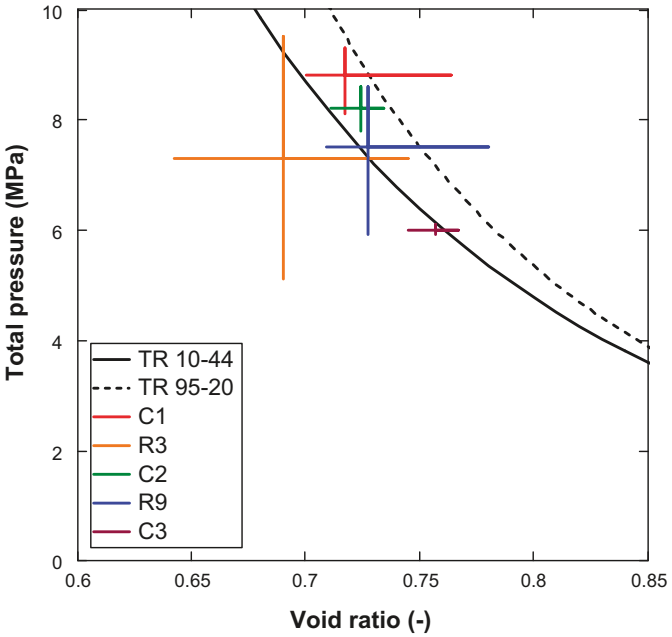

Figure 7-2. *Compilation of final pressures (minimum, mean, maximum) for each instrumented block versus the corresponding void ratios at dismantling (minimum, mean, maximum). Two swelling pressure curves shown for comparison.*

Validity of the material models

The following conclusions were made from the assessments of the validity of the material models.

The results from the *thermal model* were generally in good agreement with experimental data. However, the ABAQUS model under-predicted the temperatures in the central parts of the lower package, while the UPC CODE_BRIGHT models of the lower package over-predicted the temperatures in the peripheral parts. Still, these deviations appeared to be caused by the geometry and boundary conditions, rather than by limitations in the material model.

For the *TH-model* the following four observations were made: i) Experimental data could be reproduced to a limited extent, if uncertainties were addressed and the flow coefficients as well as the retention properties were varied within relevant bounds. ii) The hydration process around the upper heater, with moderate temperatures, could be fairly well reproduced with the material model adopted for CODE_BRIGHT, whereas the corresponding process around the lower heater, with very high temperatures, tended to exaggerate the dehydration and delay the re-saturation process. This was essentially the result from both teams using CODE_BRIGHT. The ABAQUS model displayed a better agreement, but in order to achieve this it was necessary to effectively halve the vapor diffusivity coefficient. iii) Early RH-evolution and pore-pressures (if accurate) in the lower package could not be reproduced with current constitutive laws. iv) investigations of fundamental mechanism for supporting different constitutive laws and parameters values would be valuable.

For the *mechanical model*, the following five observations were made: i) Swelling pressures, i.e. the relation between the void ratio and net mean stress during the final state, could be well reproduced with the material model developed for the SR-Site (i.e. for THM modelling with CODE_BRIGHT at Clay Technology) (Figure 7-3). This was facilitated by the inbuilt swelling pressure relation in the kappa_s function. ii) The plastic parameters describing the yield surface is highly related to the void ratio. The yield surface is however (according to the BBM) unaffected during swelling at fairly isotropic stress states. The current approach (for THM modelling with CODE_BRIGHT at Clay Technology) to adopt plastic parameters for swelling materials (i.e. highly compacted blocks) has therefore been to set the parameter values for a target void ratio representing totally homogenized conditions. This approach was improved in this modelling task, through the adoption of a LC-curve included in the BBM. The void ratio dependence of the yield surface could in this way be mimicked by a suction dependence of the yield surface. iii) Calculated von Mises stresses were in some cases

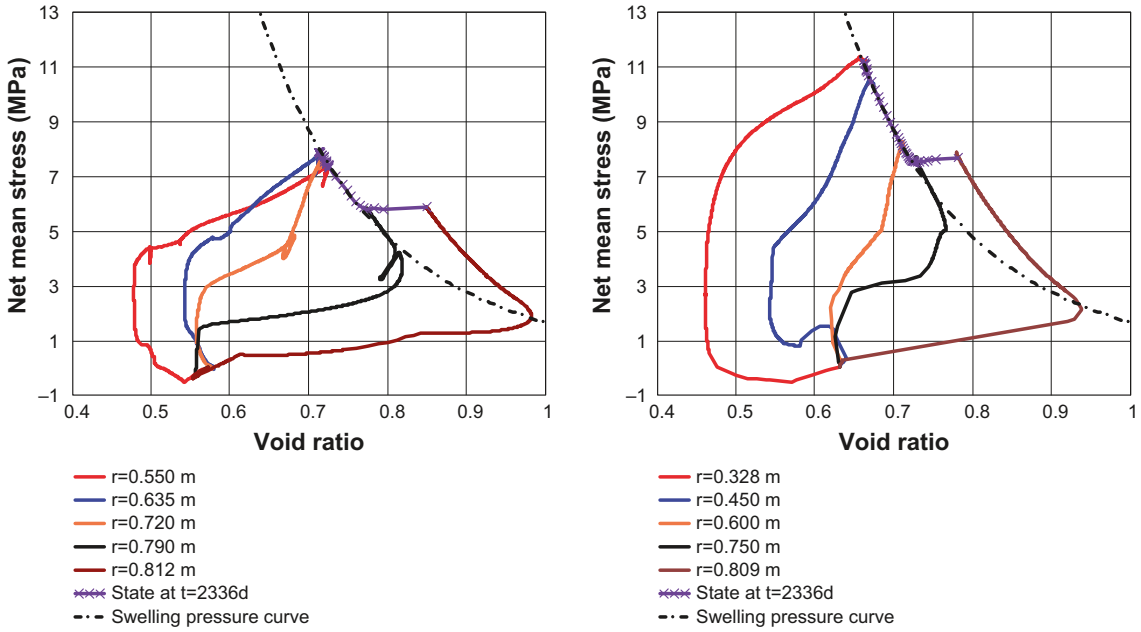

Figure 7-3. *Stress paths for different radii and final state in numerical models together with adopted swelling pressure curve. Left graph shows results for model of the upper package (TBTR10A2). Right graph shows results for model of the lower package (TBTR4_THMg_A1).*

significantly lower than the experimental data (Figure 7-4). This suggested that the shape of the actual yield surface was different than the shape implied by the modified Cam-Clay surface included in the BBM. iv) General evolution of stresses has been fairly well mimicked by the ABAQUS contribution, using a porous elastic model with moisture swelling and Drucker Prager. The void ratios around upper heater, as well as the cable forces and the lid displacements were also well reproduced. v) The CODE_BRIGHT models presented by UPC (using BBM or BExM) showed that the general evolution of stresses could be fairly well mimicked, although the deviatoric stresses around the upper heater were under-predicted. The final dry-density distribution around both heaters could also be fairly well reproduced.

The *thermal expansion of water* was treated as a constant in the used codes. The default values were representative for temperatures at around 30°C and were therefore inadequate for TBT conditions. The ClayTechnology contribution using CODE_BRIGHT demonstrated however that this could to some extent be compensated by adopting a higher parameter value. One phenomenon which should be influenced by the thermal expansion is the occurrence of pressure drops at occasions with decreasing temperatures. This process is however not really captured with the current constitutive laws, and the prospects is therefore currently small for reproduction of such pressure drops in a consistent way.

The inclusion of *gas transport* is necessary for conditions with temperatures exceeding 100°C for codes with explicit representation of water vapor. In addition, the inclusion of gas generally enhances the vapor transport. Both modelling teams using CODE_BRIGHT have included the gas transport in all models with temperatures exceeding 100°C. Gas transport was however not considered in the ABAQUS model. The experimental data suggested that TBT was influenced by a gas escape route, which limited the gas pressure in the sand shield to an atmospheric level. This condition could be sustained until the shield was filled with water. In addition, this gas escape route may also have limited the gas pressure in the lower package. This notion is to some extent supported by results from numerical models. Moreover, the inherent model behavior, with parallel gradients of the gas pressure profile and the temperature profiles, is quite counterintuitive. It would therefore be valuable to investigate the fundamental mechanism behind this process together with the general TH model.

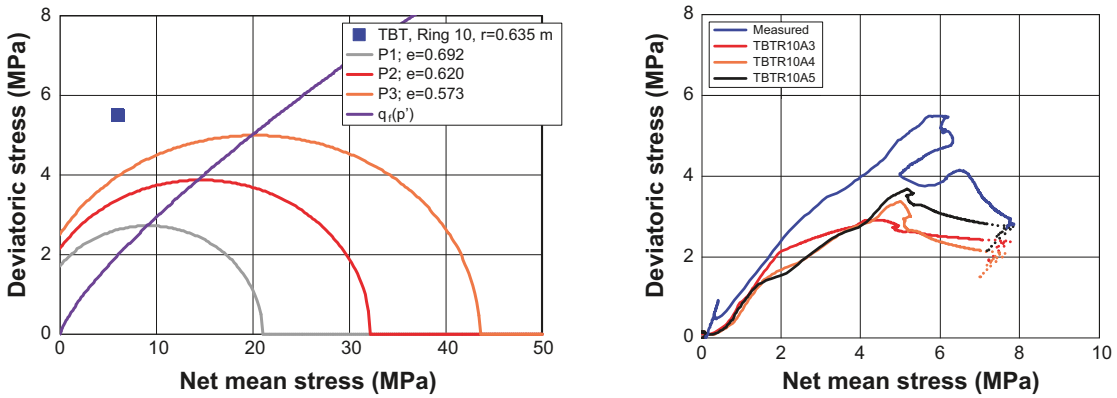

Figure 7-4. *Yield surfaces for the three different plastic parameter sets to the left and deviatoric stress vs. net mean stress evolution at r = 0.635m in Ring 9 to the right. The blue square in the left panel is the point in p'-q space where the bentonite plasticized in TBT, a point which none of the yield surfaces used in the modelling can reproduce.*

The employment of *sand compressibility* values from independent oedometer tests resulted in over-estimated stress levels. This was essentially the conclusion for all the modelling teams. This could be a consequence of the 1D geometry, by which no axial strains was allowed. The experimental results suggested that the axial strains were significant in Ring 3, Ring 4 as well as in Ring 10, but not in Ring 9. An alternative explanation could be that the independent oedometer tests tended to underestimate the compressibility of the sand.

The friction along the rock wall is of importance for reproducing the balance between the cable forces and the swelling pressures. The magnitude of this force component could to some extent be evaluated from the experimental data and this force was supported by the results from the ABAQUS model which also could reproduce the evolution of the cable forces. It was however not possible to reproduce this force balance with the CODE_BRIGHT models.

8 Remarks on test design

Two test design features which are not part of the KBS-3 concept, i.e. the sand shield and the sand filter, have been employed in the TBT. The motive behind the shield was that it would improve the possibility to retrieve a canister, and also that it would act as a thermal protection for the bentonite buffer. The intention with the sand filter was that this would be an efficient and robust technique for supplying water to the bentonite. The function of these two sand-filled slots is discussed in this final chapter.

The mechanical properties of the sand used in the sand-filled slots are of importance for the THM modelling. For instance, calculated swelling pressures tended to be overestimated in models in which independent determined oedometer module values were used. This may be an effect of axial swelling of the bentonite, and this is to some extent supported by the experimental data, but an alternative explanation could be that the independent oedometer tests tend to underestimate the compressibility of the sand. Moreover, the measurements of the inner radii of the rings around the sand shield indicated that the radial inward swelling was more pronounced in the lower part of the shield than in the upper part (see Figure 4-3). This type of behavior appears to be very difficult to capture with the current THM tools. Finally, the plastic properties of the sand appear to have enabled the formation of a gap between the bentonite and the sand filter during the cooling of the experiment. This gap, in turn, enabled an extensive water uptake and swelling in the outer part of the blocks. Taken together, the inclusion of the sand-filled slots implied that the experiment became mechanically more complex, which meant that additional uncertainties were introduced in the THM modelling.

Water injection has been one of the main functions of the sand-filled slots. This is obvious for the filter, but water injection was also an important aspect for the shield. In fact, the shield hydration was the main concern for the project operators during a five months period in 2007/2008. In general, the hydraulic properties of the sand have appeared to be quite suitable for water injection. The pore pressures levels at different locations of the filter were basically the same which indicated that the flow resistance of the sand was negligible. However, the use of filter tips has been a source of a number of difficulties. The filter tips in the sand filter were covered with calcite precipitates when formation water was injected. This increased the flow resistance of the filter tips to such an extent that it became impossible to sustain any significant pore pressures in the filter. This fact motivated the change in water quality from formation water to the use of deionized water. The injection system into the sand shield also exhibited a high flow resistance, but in this case it appeared to be caused by swelling bentonite which thereby could cover the filter tips in the sand shield.

Some of the *fractures observed in the bentonite blocks* may have been caused by the use of sand-filled slots. Three types of fractures were observed during the dismantling operation: i) the fairly horizontal or slightly dome-shaped fractures that were found in virtually all blocks in the lower package; ii) the fallout of “chevron-shaped” pieces from Ring 10 – Ring 7; and iii) a number of observations that suggest that an upward swelling of Ring 12 had sheared the outer parts of Cylinder 3. The cause of the fairly horizontal fractures is currently unknown, and it is therefore uncertain if these are related to the sand-filled slots. The fallout of pieces from the upper package may be caused by the unloading of the bentonite during the removal of the shield sand. These fractures could however be formed much earlier, and this is supported by the occurrence of very high von Mises stresses in Ring 9 at around day 200. The combination of a high block dry density and the possibility to swell in radial direction appears to be the cause of such high von Mises stresses. Such conditions are however not unique for the TBT with sand-filled slots, and may also be present in an KBS-3 buffer. Finally, the upward swelling of Ring 12 and the shearing of the outer part of Cylinder 3 appears to be related to the sand filter. The sand filling of the outer slot was replaced by the pellets filling at the mid-section of Ring 12. This implied that all bentonite below this level had free access of water, whereas the bentonite above it had very limited access. Large shearing event may occur under such conditions, in which the rate of swelling pressure build-up is different in different sections. This type of fracture therefore appears to be quite unique for the TBT design, although it shouldn’t be ruled out that a similar process could take place in a KBS-3 buffer at conditions with localized water entry.

9 References

SKB's (Svensk Kärnbränslehantering AB) publications can be found at www.skb.se/publications.

Andersson C, Johansson Å, 2002. Boring of full scale deposition holes at the Äspö Hard rock Laboratory. Operational experiences including boring performance and a work time analysis. SKB TR-02-26, Svensk Kärnbränslehantering AB.

Bäck R, 2002. Äspö Hard Rock Laboratory. Temperature Buffer Test. Report for retaining plug and anchoring. SKB IPR-02-64, Svensk Kärnbränslehantering AB.

Börgesson L, 2002. Äspö Hard Rock Laboratory. Temperature Buffer Test. Data management. SKB IPR-03-11, Svensk Kärnbränslehantering AB.

Fälth B, Börgesson L, Hökmark H, Hernelind J, 2005. THM predictive modeling of the Temperature Buffer Test – Clay Technology's contribution. In Alonso E E, Ledesma A (eds). Advances in understanding engineered clay barriers: proceedings of the International Symposium on Large Scale Field Tests in Granite, Sitges, Barcelona, Spain, 12–14 November 2003. Rotterdam: Balkema, 461–482.

García-Siñeriz J L, Fuentes-Cantillana J L, 2002. Äspö Hard Rock Laboratory. Temperature Buffer Test. Feasibility study for the heating system at the TBT test carried out at the Äspö HRL in Sweden. SKB IPR-03-18, Svensk Kärnbränslehantering AB.

Goudarzi R, Börgesson L, Sandén T, Barcena I, 2003. Äspö Hard Rock Laboratory. Temperature Buffer Test. Sensors data report (Period 030326–031001) Report No:1. SKB IPR-04-02, Svensk Kärnbränslehantering AB.

Goudarzi R, Börgesson L, Sandén T, Barcena I, 2004a. Äspö Hard Rock Laboratory. Temperature Buffer Test. Sensors data report (Period 030326–040101) Report No:2. SKB IPR-04-14, Svensk Kärnbränslehantering AB.

Goudarzi R, Börgesson L, Hökmark H, 2004b. Äspö Hard Rock Laboratory. Temperature Buffer Test. Sensors data report (Period 030326–040401) Report No:3. SKB IPR-04-29, Svensk Kärnbränslehantering AB.

Goudarzi R, Börgesson L, Hökmark H, 2004c. Äspö Hard Rock Laboratory. Temperature Buffer Test. Sensors data report (Period 030326–040701) Report No:4. SKB IPR-04-49, Svensk Kärnbränslehantering AB.

Goudarzi R, Åkesson M, Hökmark H, 2005a. Äspö Hard Rock Laboratory. Temperature Buffer Test. Sensors data report (Period 030326–050101) Report No:5. SKB IPR-05-06, Svensk Kärnbränslehantering AB.

Goudarzi R, Åkesson M, Hökmark H, 2005b. Äspö Hard Rock Laboratory. Temperature Buffer Test. Sensors data report (Period 030326–050701) Report No:6. SKB IPR-05-20, Svensk Kärnbränslehantering AB.

Goudarzi R, Åkesson M, Hökmark H, 2005c. Äspö Hard Rock Laboratory. Temperature Buffer Test. Sensors data report (Period 030326–060101) Report No:7. SKB IPR-06-04, Svensk Kärnbränslehantering AB.

Goudarzi R, Åkesson M, Hökmark H, 2006. Äspö Hard Rock Laboratory. Temperature Buffer Test. Sensors data report (Period 030326–060701) Report No:8. SKB IPR-06-27, Svensk Kärnbränslehantering AB.

Goudarzi R, Åkesson M, Hökmark H, 2007a. Äspö Hard Rock Laboratory. Temperature Buffer Test. Sensors data report (Period 030326–070101) Report No:9. SKB IPR-07-07, Svensk Kärnbränslehantering AB.

Goudarzi R, Åkesson M, Hökmark H, 2007b. Äspö Hard Rock Laboratory. Temperature Buffer Test. Sensors data report (Period 030326–070701) Report No:10. SKB IPR-07-21, Svensk Kärnbränslehantering AB.

Goudarzi R, Åkesson M, Hökmark H, 2008a. Äspö Hard Rock Laboratory. Temperature Buffer Test. Sensors data report (Period 030326–080101) Report No:11. SKB IPR-08-16, Svensk Kärnbränslehantering AB.

Goudarzi R, Åkesson M, Hökmark H, 2008b. Äspö Hard Rock Laboratory. Temperature Buffer Test. Sensors data report (Period 030326–080701) Report No:12. SKB IPR-09-04, Svensk Kärnbränslehantering AB.

Goudarzi R, Åkesson M, Nilsson U, 2010. Temperature Buffer Test. Sensors data report (Period 030326–100301) Report No:13. SKB P-12-03, Svensk Kärnbränslehantering AB.

Hardenby C, 2002. Äspö Hard Rock Laboratory. Tunnel for the canister retrieval test. Geological mapping of tunnel and deposition holes. SKB IPR-02-49, Svensk Kärnbränslehantering AB.

Hökmark H, 2005. Temperature Buffer Test – comparison of modeling results/experimental findings: causes of differences. In Alonso E E, Ledesma A (eds). Advances in understanding engineered clay barriers: proceedings of the International Symposium on Large Scale Field Tests in Granite, Sitges, Barcelona, Spain, 12–14 November 2003. Rotterdam: Balkema, 373–390.

Hökmark H, Börgesson L, Hernelind J, 2005. Äspö Hard Rock Laboratory. Temperature Buffer Test. Scoping design calculations. SKB IPR-05-07, Svensk Kärnbränslehantering AB.

Hökmark H, Ledesma A, Lassabatere T, Fälth B, Börgesson L, Robinet J C, Sellali N, Sémété P, 2007. Modelling heat and moisture transport in the ANDRA/SKB temperature buffer test. Physics and Chemistry of the Earth, Parts A/B/C 32, 753–766.

Johannesson L-E, 2010. Temperature Buffer Test. Measurements of water content and density of the excavated buffer material. SKB P-12-05, Svensk Kärnbränslehantering AB.

Johannesson L-E, Sandén T, Åkesson M, Bárcena I, Garzía-Siñeriz, 2010. Temperature Buffer Test. Installation of buffer, heaters and instruments in the deposition hole. SKB P-12-02, Svensk Kärnbränslehantering AB.

Karlsson T, 2002. Äspö Hard Rock Laboratory. Temperature Buffer Test. Report for data acquisition equipment. SKB IPR-03-12, Svensk Kärnbränslehantering AB.

Sandén T, Goudarzi R, de Combarieu M, Åkesson M, Hökmark H, 2007. Temperature Buffer Test – design, instrumentation and measurements. Physics and Chemistry of the Earth, Parts A/B/C 32, 77–92.

Thorsager P, 2002. Äspö Hard Rock Laboratory. Temperature Buffer Test. Detailed design materials. Foundation and artificial saturation. SKB IPR-02-62, Svensk Kärnbränslehantering AB.

Åkesson M (ed), 2006a. Äspö Hard Rock Laboratory. Temperature Buffer Test. Evaluation modeling – Field test. SKB IPR-06-10, Svensk Kärnbränslehantering AB.

Åkesson M (ed), 2006b. Äspö Hard Rock Laboratory. Temperature Buffer Test. Evaluation modeling – Mock-up test. SKB IPR-06-11, Svensk Kärnbränslehantering AB.

Åkesson M (ed), 2008. Äspö Hard Rock Laboratory. Temperature Buffer Test. Evaluation modeling. TBT_3 Mock-up test. SKB IPR-08-09, Svensk Kärnbränslehantering AB.

Åkesson M, 2010. Temperature Buffer Test. Dismantling operation. SKB P-12-04, Svensk Kärnbränslehantering AB.

Åkesson M, Jacinto A, Gatabin C, Sanchez M, Ledesma A, 2009. Bentonite THM behaviour at high temperatures: experimental and numerical analysis. Géotechnique 59, 307–318.

Åkesson M, Olsson S, Dueck A, Nilsson U, Karnland O, Kiviranta L, Kumpulainen S, Lindén J, 2012a. Temperature Buffer Test. Hydro-mechanical and chemical/mineralogical characterizations. SKB P-12-06, Svensk Kärnbränslehantering AB.

Åkesson M, Malmberg D, Börgesson L, Hernelind J, Ledesma A, Jacinto A, 2012b. Temperature Buffer Test. Final THM modelling. SKB P-12-07, Svensk Kärnbränslehantering AB.